

## Article

# Synthesis of Gum Arabic Magnetic Nanoparticles for Adsorptive Removal of Ciprofloxacin: Equilibrium, Kinetic, Thermodynamics Studies, and Optimization by Response Surface Methodology

Abdullahi Haruna Birniwa <sup>1</sup>, Rania Edrees Adam Mohammad <sup>2,3,\*</sup>, Mujahid Ali <sup>4,\*</sup>,  
Muhammad Faisal Rehman <sup>5</sup>, Shehu Sa'ad Abdullahi <sup>6</sup>, Sayed M. Eldin <sup>7</sup>, Suwaiba Mamman <sup>8</sup>,  
Abubakar Chadi Sadiq <sup>9</sup> and Ahmad Hussaini Jagaba <sup>10</sup>

- <sup>1</sup> Department of Chemistry, Sule Lamido University, Kafin-Hausa PMB 048, Nigeria  
<sup>2</sup> School of Chemical Sciences, Universiti Sains Malaysia, Pulau Pinang 11800, Malaysia  
<sup>3</sup> Faculty of Education, Sciences Department, Open University of Sudan, Khartoum 13091, Sudan  
<sup>4</sup> Department of Civil Engineering, Faculty of Engineering, Universiti Malaya, Kuala Lumpur 50603, Malaysia  
<sup>5</sup> The Department of Architecture, University of Engineering and Technology, Peshawar 473226, Pakistan  
<sup>6</sup> Department of Polymer Technology, Hussaini Adamu Federal Polytechnic, Kazaure PMB 5004, Nigeria  
<sup>7</sup> Center of Research, Faculty of Engineering, Future University in Egypt, New Cairo 11835, Egypt  
<sup>8</sup> Department of Chemistry, Faculty of Natural and Applied Sciences, Nasarawa State University, Keffi PMB 1022, Nigeria  
<sup>9</sup> Department of Chemistry, Faculty of Science, Bauchi State University, Gadau PMB 065, Nigeria  
<sup>10</sup> Department of Civil Engineering, Abubakar Tafawa Balewa University, Bauchi PMB 0248, Nigeria  
\* Correspondence: raniamoooc@gmail.com (R.E.A.M.); s2040165@siswa.um.edu.my (M.A.);  
Tel.: +601-8838-919 (R.E.A.M.)



**Citation:** Birniwa, A.H.; Mohammad, R.E.A.; Ali, M.; Rehman, M.F.; Abdullahi, S.S.; Eldin, S.M.; Mamman, S.; Sadiq, A.C.; Jagaba, A.H. Synthesis of Gum Arabic Magnetic Nanoparticles for Adsorptive Removal of Ciprofloxacin: Equilibrium, Kinetic, Thermodynamics Studies, and Optimization by Response Surface Methodology. *Separations* **2022**, *9*, 322. <https://doi.org/10.3390/separations9100322>

Academic Editors: Amin Mojiri and Mohammed J.K. Bashir

Received: 21 September 2022

Accepted: 14 October 2022

Published: 21 October 2022

**Publisher's Note:** MDPI stays neutral with regard to jurisdictional claims in published maps and institutional affiliations.



**Copyright:** © 2022 by the authors. Licensee MDPI, Basel, Switzerland. This article is an open access article distributed under the terms and conditions of the Creative Commons Attribution (CC BY) license (<https://creativecommons.org/licenses/by/4.0/>).

**Abstract:** Given the increasing risks that antibiotic abuse poses to microecology and human health, it is imperative to develop incredibly powerful adsorbents. This study investigated the use of environmentally sustainable polymeric nanocomposite based on gum arabic (GA) and magnetic nanoparticles (MNPs) synthesized via co-precipitation method to form gum arabic magnetite nanoparticles (GA-MNPs) as an efficient adsorbent for ciprofloxacin (CIP) removal from aqueous solution. The physicochemical properties and morphology of the synthesized GA-MNPs were characterized by Fourier transform infrared spectroscopy (FTIR), scanning electron microscopy (SEM), and Energy Dispersive X-Ray Analysis (EDX). The experiment was designed by response surface methodology (RSM) and the Central Composite Design (CCD) was utilized to optimize the operating variables: contact time (0–120 min), pH (3–10), adsorbent dosage (0.10–0.40 g/L), and concentration of adsorbate (5–100 mg/L). Results showed that 96.30% was the maximum percentage of CIP removed. The adsorption effect of the CIP molecule on the surface of the GA-MNPs was investigated using regression analysis and analysis of variance. Furthermore, Freundlich Isotherm and Pseudo Second order kinetic equations have the highest consistency with experimental investigations suggesting double-layer adsorption. This implies that chemisorption was the mechanism involved. In addition, the calculated thermodynamic parameters were postulating an exothermic and spontaneous method in nature. Owing to its adsorption selectivity and recyclability, GA-MNPs could be classified as an environmentally friendly, less expensive, and highly efficient promising adsorbent for remediation of CIP from aqueous solution.

**Keywords:** adsorption; central composite design; ciprofloxacin; gum arabic magnetite; response surface methodology; wastewater

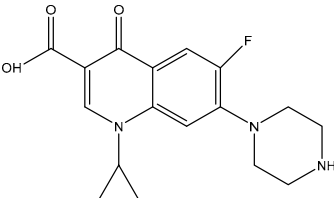
## 1. Introduction

Water is the most abundant and compulsory component required for the existence of living organisms on the planet [1]. The accessibility of potable water remains a great

challenge for over a decade due to the global discharge of environmental effluents caused by the increase in unprecedented population growth, urbanization, and industrialization [2,3]. Thus, to achieve one of the targets of the Sustainable Development Goal (SDG 6) set by the United Nations General Assembly by the year 2030, outstanding techniques and materials need to be established to guarantee access to clean water for all [4].

The increased health risk caused by the random disposal of pharmaceuticals in aqueous medium has caused serious problems owing to their negative impacts on the environment [5,6]. This is because pharmaceuticals are only partly metabolized in the human body after ingestion, with 20–80% of the unmetabolized residues being discharged into the environment in a pharmacologically active form. Numerous pharmaceutical active compounds are directly or indirectly released into the environment [7,8]. However, domestic waste, hospital waste, pharmaceutical industry by-products, and human urine are the main sources of drug contamination [9,10]. The vital antibacterial agents utilized in human and veterinary medicine are fluoroquinolone antibiotics [11–14]. Ciprofloxacin (CIP) is a wide antibiotic spectrum that is extensively used to prevent post-operative infection following intra-abdominal surgery [15,16], the characteristics of which are presented in Table 1. A wide range of approaches have been used for the removal of CIP from various water sources. These include: photodegradation [17,18], ozonation, photo-Fenton [19], Fenton oxidation process [20], and adsorption. Antibiotics can be effectively removed from the aqueous solution via an adsorption process [13,21]. To date, various adsorbents for CIP removal such as titanium carbide [22], humic acid coated magnetic biochar [23], nano-hydroxyapatite [24], multiwall carbon nanotube [25], activated carbon, montmorillonite [26], and Graphene oxide [27] have been recorded. However, some of these adsorbents are highly expensive, toxic, and difficult to regenerate after use. Therefore, an ecofriendly, less expensive, easy to recover, biocompatible, and less toxic adsorbents need to be produced. Natural supporting adsorbents from plant sources such as Gum Arabic (GA) can be explored.

**Table 1.** CIP physical composition and chemical structure [21].

Parameters	CIP
Molecular structure	
Formula	C <sub>17</sub> H <sub>18</sub> FN <sub>3</sub> O <sub>3</sub>
Family	Fluoroquinolone
Molecular weight (g/mol)	331.346
pKa	5.76–8.68
Log P	−0.81

GA is a natural polysaccharide produced from *Acacia Senegal* and *Acacia Seyal* exudates [28,29]. It is an inexpensive, hydrophilic, non-toxic, biocompatible, fully biodegradable polymer [30–32]. GA mostly comprises a polysaccharide with several branches containing rhamnose, arabinose, and galactose, a lesser fraction of arabinogalactan–protein complex, and the minimum fraction of glycoprotein [33–35]. Recently, GA has gained great attention as an appropriate biomaterial candidate owing to its biological, chemical, and physical characteristics [36,37]. GA special features enables it to be a promising material in a variety of fields in recent years [38]. It has been highlighted as an important dispersion for carbon nanotubes as well as for removing copper ions from aqueous solutions using a nano-adsorbent coating material [39,40]. Moreover, it has been proven that GA can stabilize iron oxide nanoparticle dispersions in aqueous media [38]. As an active base, it may be used to create stable colloidal nanoparticles that have external reactive functional groups [41].

Similarly, it has been applied to stabilize and functionalize nanoparticles [8]. Recently, it was revealed that GA-modified magnetite nano-adsorbents could produce magnetic hyperthermia and were very successful at removing lead from wastewater [42,43].

Magnetic nanoparticles (MNPs) are a new class of nano-adsorbents that comprises magnetic elements, such as nickel, iron, and cobalt [36]. MNPs modified surface chemistry using natural or synthetic polymers have been widely used in several fields [44]. The fundamental properties of nanoparticles such as a high surface area to volume ratio, small size, and absence of internal diffusion resistance, gives outstanding adsorption kinetics of the contaminants from aqueous solutions. MNPs have the advantages of both magnetic separation techniques and nano-sized materials, which can be recovered easily or removed with an external magnetic field [45,46]. Several coating agents have been employed to develop biocompatible, monodisperse, and stable MNP suspensions [47]. A few literature studies have discussed the use of GA-MNPs for the adsorption of certain wastewater contaminants. Saeed et al. [48] reported the removal effects of GA-coated MNPs for the removal of Pb ions from aqueous solutions. A study by Movasaghi et al. [49] reported the use of Gum MNPs as an eco-friendly adsorbent for the removal of lead (II) Ions from aqueous solutions with a maximum adsorption capacity of 50.5 mg/g. Moreover, in another research study, the removal of methylene blue dye using GA/MNPs from synthetic wastewater achieved the maximum adsorption capacity of 38.5 mg/g [50].

In this study, the synthesis and characterization of stable and porous GA-MNPs for efficient CIP removal in an aqueous medium was explored. The central composite design (CCD) in the response surface methodology (RSM) was utilized to produce experimental models suitable for design, prediction, and validation to generate optimum runs that are significant for determining CIP adsorption/desorption. Subsequently, the langmuir, freundlich, temkin, and dubinin-radushkevich isotherm models were used for data analysis. More so, the pseudo-first order, pseudo-second order, intraparticle diffusion, elovich, kinetic models, and thermodynamic parameters were studied.

## 2. Materials and Methods

### 2.1. Materials and Reagents

Ciprofloxacin (97–100% purity) was acquired from Sigma-Aldrich (Darmstadt, Germany). Gum Arabic, Iron (III) Chloride hexahydrates, Ammonium iron (II) sulfate hexahydrate, ethanol, Ammonia solution (28%) were utilized for the study. All other chemicals were used without further purification and obtained as analytical grade products [51].

### 2.2. Instrumentations

GA, GA-MNP functional groups, and morphology were studied using FTIR and SEM/EDX techniques. The Thermo Scientific, Waltham, MA, USA (NICOLET iS10) was used to acquire the FTIR functional groups of the samples in the region of 4000–400  $\text{cm}^{-1}$  at room temperature. The SEM/EDX method was used to analyze the morphology of GA and GA-MNP (FESEM Model SU 8220, Hitachi, Japan). The UV-VIS spectrophotometer coupled with 10 mm quartz cuvettes was used for the quantification of CIP.

### 2.3. Synthesis of Gum Arabic Magnetite Nanoparticles (GA-MNPs)

A one-step process with numerous improvements was adopted for the synthesis of GA coated  $\text{Fe}_3\text{O}_4$  as illustrated in Figure 1 [46]. 100 mL of deoxygenated water was used as a solvent to dissolve 2.0 g  $\text{FeCl}_2 \cdot 4\text{H}_2\text{O}$  and 5.2 g  $\text{FeCl}_3 \cdot 6\text{H}_2\text{O}$ . 2.0  $\text{g L}^{-1}$  GA was dissolved in 50 mL deionized water and added to the mixture with continuous stirring at 80 °C under  $\text{N}_2$  stream. Subsequently, ammonium hydroxide (28%) was drop-wise into the reaction mixture until pH 10. After maintaining the mixture at 80 °C for 60 min, it was allowed to cool down. The GA-MNPs was finally separated magnetically and washed with absolute ethanol and distilled water for several time.

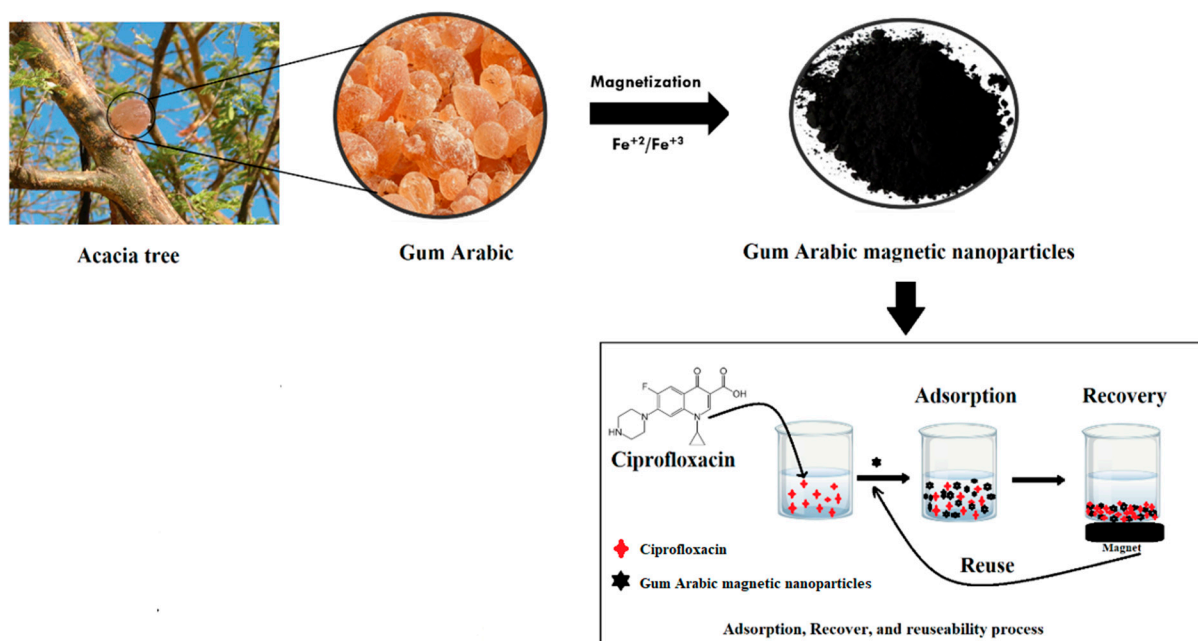


**Figure 1.** Synthesis of Gum Arabic Magnetite and the adsorption study process.

*2.4. Batch Adsorption Experiment*

20 mg of GA-MNPs adsorbent was added to 20 mL of aqueous solution that contained 10 mg/L of CIP. Then, the mixture was shaken using an orbital shaker at 250 rpm at 25 °C for 30 min. After adsorption, an external magnet was subjected to separate the adsorbents from the solution. The mixture undergoes a quantitative analysis using a UV-VIS spectrophotometer at 227 nm. The effect of variables such as pH, contact time, temperature, adsorbent dosage, and CIP initial concentration were studied. Equations (1) and (2) were adopted to obtain the removal (R%) and adsorption capacity (q) of the CIP, respectively [24,50]:

$$\text{Removal efficiency (\%)} = \frac{(C_0 - C_f)}{C_0} \times 100 \tag{1}$$

$$q_e = \frac{[(C_0 - C_f) \times v]}{w} \tag{2}$$

From the equations, the initial CIP concentration is represented with C<sub>0</sub> (ppm), C<sub>f</sub> (ppm) represents the CIP equilibrium concentration, v (L) represents the quantity of adsorbent, and v (L) is the solution volume.

The material has been regenerated, washed with deionized water and methanol, and dried in an oven for six hours prior to reuse.

*2.5. Response Surface Methodology (RSM)*

RSM is a multivariate statistical and mathematical procedure that can be applied to the model to understand and give an experimental insight when a response of significance is determined by multiple variables. The target is to optimize the response. The CCD requires fewer experimental runs but produces the same set of data as the 3n complete factorial design. The CCD is surrounded by axial points, a two-level factorial design with a center point that corresponds to the middle level of the factors, and axial points (2n). The number of axial points (2n) depends on the number of parameters linked to the desired features of the design [52]. Due to the location of the axial points, the CCD may be divided into three groups: CCC (circumscribed central composite), CCI (inscribed central composite), and CCF (face centered composite). Comparing the region of operability with the region

of interest is crucial when choosing the proper type of CCD. CCD is the most widely used technique for creating second-order response models for environmental applications. It offers sequential strategic experiments and can be effectively employed for up to five parameters using parallel experiments. Additionally, it can significantly forecast the effects of linear and quadratic interactions and optimize a huge number of variables.

The RSM employed in this work was a CCD with five independent variables: a dose of GA-MNPs, contact time, pH, CIP concentration, and temperature. Table 2 lists the variables and their respective levels. The five-coded scale was used to evaluate the input values ( $-\alpha$ , low, center, high, and  $+\alpha$ ). CIP removal was the target of the experiments. Five process variables that could effectively remove CIP were considered. A total of 50 sets of trials were used with  $2^5$  full factorial designs. A total of 32 trials for factorial point design, 10 for axial point, and 8 for a facsimile of the midpoint were included in the CCD experimental set of 50 trials. Design Expert Software (11 trial versions, Stat Ease, Minneapolis, MN, USA) was used to analyze the outcomes in more detail.

**Table 2.** RSM matrix for the optimization of CIP removal.

Independent Variables	Symbol	Ranges and Codes				
		$-\alpha$	Low	Centre	High	$+\alpha$
pH	$k_a$	2	4	6	8	10
CIP concentration (ppm)	$k_b$	20	40	60	80	100
Temperature ( $^{\circ}\text{C}$ )	$k_c$	25	35	45	55	65
GA-MNPs dose (g)	$k_d$	10	20	30	40	50
Contact time (min)	$k_e$	24	48	72	96	120

The implications of the model were evaluated using analyses of variance (ANOVA) attributed to the determination coefficient, Fischer’s value test (F-value), and the value of probability ( $p$ -value). The ANOVA program from Design Expert was applied to fully evaluate the outcomes. Based on the interaction between the levels of the five variables, plots of three-dimensional and their corresponding contour plots were produced. The model was described by Equation (3).

$$f(m) = \beta_0 + \sum_{u=1}^w \beta_u m_u + \sum_{i=1}^w \sum_{v \geq i}^w \beta_{uv} m_u m_v + \zeta \tag{3}$$

where  $m_u$  and  $m_v$  are independent variables,  $\beta_0$ ; constant,  $\beta_u$ ; linear coefficient and  $\beta_{uv}$ ; interactive coefficient,  $u$ ; linear coefficient,  $v$ ; quadratic coefficient,  $y$ ; predicted response and  $\zeta$ ; noise or error detected in the reply.

**2.6. Adsorption Kinetics**

To determine the most effective kinetic model, the data for the batch adsorption study were studied via pseudo-first order, pseudo-second order, Elovich, and intra-particle diffusion, as indicated by Equations (4)–(7), respectively [53].

$$\ln(q - q_t) = \ln q_e - k_1 \tag{4}$$

$$\frac{t}{q_t} = \left( \frac{t}{k_2 q_e^2} \right) + \left( \frac{1}{q_e} \right) \tag{5}$$

$$q_t = \frac{1}{\beta} \ln(\alpha\beta) + \frac{1}{\beta} \ln t \tag{6}$$

$$q_t = Kt^{1/2} + C \tag{7}$$

The amount of sorbent adsorbed  $q_t$  (mol g<sup>-1</sup>) at time  $t$ ,  $K_1$  (min<sup>-1</sup>) and  $K_2$  (g/mol/min) are the sorption rate constants acquired from the slope and intercept of linear plots of  $(q - q_t)$  versus  $t$  and  $\frac{t}{q_t}$  versus  $t$ , while  $q_e$  (mol g<sup>-1</sup>) is the quantity of sorbent adsorbed at equilibrium where  $\alpha$  (mg g<sup>-1</sup> min<sup>-1</sup>) represents the initial sorption rate,  $\beta$  is associated with the expanded surface covering and activation energy for chemisorption (mg g<sup>-1</sup>). For intra-particle diffusion, the value of  $K$  (mg g<sup>-1</sup> min<sup>-1/2</sup>) is the constant rate for intraparticle diffusion in the model, and  $C$  (mg g<sup>-1</sup>) is the intercept.

### 2.7. Adsorption Isotherms

The Langmuir, Freundlich, and Temkin models were used for the study of isotherms fitting on the adsorption data, as shown in Equations (8)–(11), respectively [54]:

$$\frac{c_e}{q_e} = \frac{1}{q_m} c_e + \frac{1}{b_L q_m} \tag{8}$$

$$\text{Log } q_e = \text{log } K_F + \frac{1}{n_F} \text{log } C_e \tag{9}$$

$$q_e = \beta_T \ln K_T + \beta_T \ln C_e \tag{10}$$

$$\ln q_e = \ln q_m - \beta E^2 \tag{11}$$

The adsorption rate  $b$  (mg L<sup>-1</sup>) and the Langmuir constants for the adsorption capacity  $q_m$  (mg g<sup>-1</sup>) are derived from the linear plot  $\frac{c_e}{q_e}$  versus  $C_e$  with  $1/q_m$  slope and intercept of  $1/bq_m$ .  $C_e$  is the adsorbate equilibrium concentration (mg L<sup>-1</sup>). The intercept value of  $\log K_F$  and slope value of  $1/n_F$  were obtained by plotting  $\log q_e$  versus  $C_e$ .  $K_F$  signifies the adsorption intensity of the adsorbate on the adsorbent material as well as the bonding energy constant. If the value of  $n_F$  is greater than one, it shows that the adsorption circumstances are favorable [48,49]. Derived from the plot of  $q_e$  versus  $\ln C_e$ ,  $K_T$  signifies the equilibrium binding constant (L mg<sup>-1</sup>),  $\beta T = RT/b$  is the Temkin isotherm constant linked to the heat of adsorption,  $T$  is the temperature in kelvin,  $R$  gas constant, and  $b$  is the Tempkin isotherm constant. The adsorption free energy per mole of the adsorbate  $E$  (J mol<sup>-1</sup>), and (mol<sup>2</sup> J<sup>-2</sup>) is the Dubinin–Radushkevich constant related to free energy.

### 2.8. Thermodynamic Studies

Thermodynamic parameters ( $\Delta H$ ,  $\Delta S$ ,  $\Delta G$ ) are derived from Equations (12) and (13) to explain the randomness, spontaneity, and nature of the sorption process:

$$\Delta G = -RT \ln k_d \tag{12}$$

$$\ln k_d = \frac{\Delta S^\circ}{R} - \frac{\Delta H^\circ}{RT} \tag{13}$$

where  $R$  (8.31 J mol<sup>-1</sup> K<sup>-1</sup>) universal gas constant,  $T$  temperature in Kelvin, and  $k_d$  (m<sup>3</sup> mol<sup>-1</sup>) concentration of adsorbate to the adsorbent ratio in equilibrium. The Van't-Hoff plot's slope and intercept of  $\ln k_d$  as a function of  $1/T$  10<sup>3</sup>, from which  $\Delta H^\circ$  and  $\Delta S^\circ$  were acquired.

## 3. Results and Discussion

### 3.1. Characterization of GA-MNPs

The FTIR spectra of GA and GA-MNPs are given in Figure 2. The spectrum of GA in Figure 2a showed the peaks at 3339, 2881, and 1607 cm<sup>-1</sup> were attributed to the –OH stretching, –CH<sub>2</sub> stretching vibration, and C-O asymmetric stretching vibrations,

respectively. The peak at  $1404\text{ cm}^{-1}$  is assigned to the wagging vibrations for  $-\text{CH}$ . The  $\text{C}-\text{O}-\text{C}$  linkage appeared at  $1062\text{ cm}^{-1}$ , where the peak at  $610\text{ cm}^{-1}$  could be assigned for the  $-\text{C}-\text{H}$  out-of-plane bending vibration. The spectrum of GA-MNPs in Figure 2b showed increased intensity for the peak at  $1620\text{ cm}^{-1}$  with a very slight shift, indicating the formation of hydrogen bonding between the GA and the MNPs. The absorption bands at  $600\text{ cm}^{-1}$  could be attributed to  $\text{Fe}-\text{O}$  bonds due to their stretching vibration mode in the crystalline lattice of GA-MNPs [49]. Moreover, the peak at  $1436\text{ cm}^{-1}$  showed an increase in intensity, indicating the interaction between the carboxylic functional group of GA and the hydroxyl group on the surface of MNPs [46]. The morphological characterization of the synthesized GA-MNPs material was analyzed using SEM. The spherical shape of the  $\text{Fe}_3\text{O}_4$  nanoparticles—which exhibited rough and agglomerated morphology due to magnetism and high surface energy—confirm the successful synthesis of MNPs as can be seen in Figure 3a. However, the surfaces of GA and GA-MNPs were smooth as depicted in Figure 3b,c. This suggests that the agglomeration decreased upon coating with GA. Figure 4. shows clear EDX peaks of C (20.57%), Fe (66.58%), and O (9.90%) in the adsorbent. This proves the successful formation of GA-MNPs and correlates with the FTIR results of the nanoparticles.

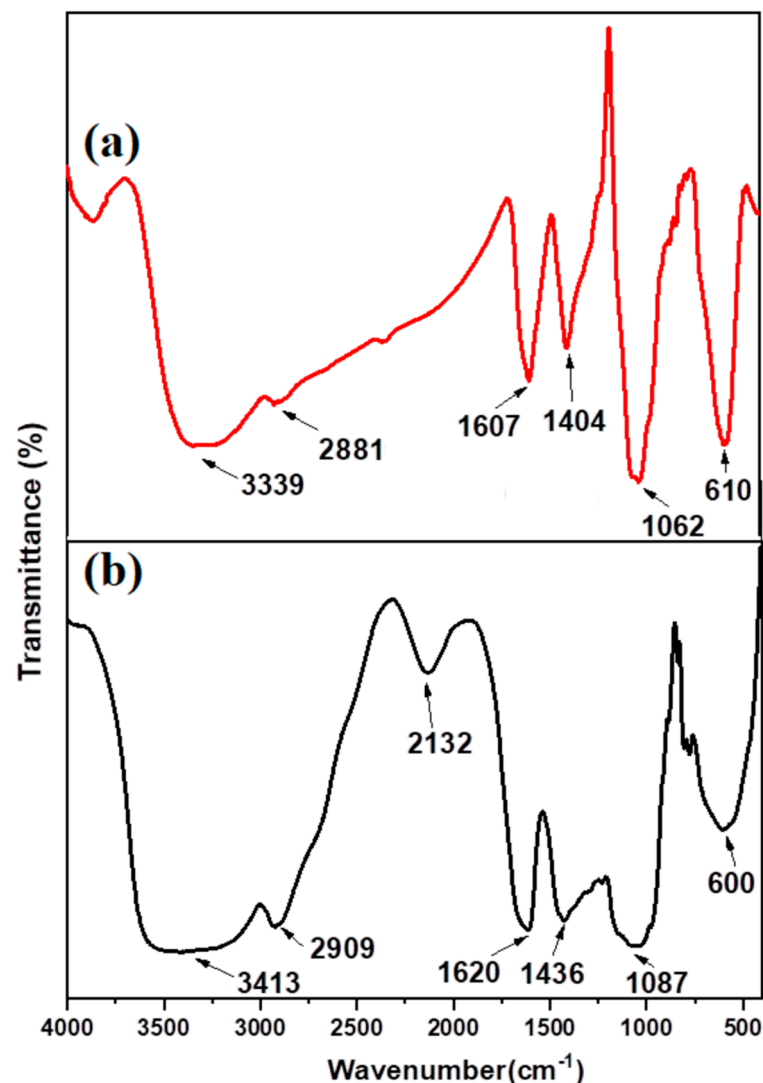


Figure 2. FTIR spectra of (a) GA and (b) GA-MNPs.

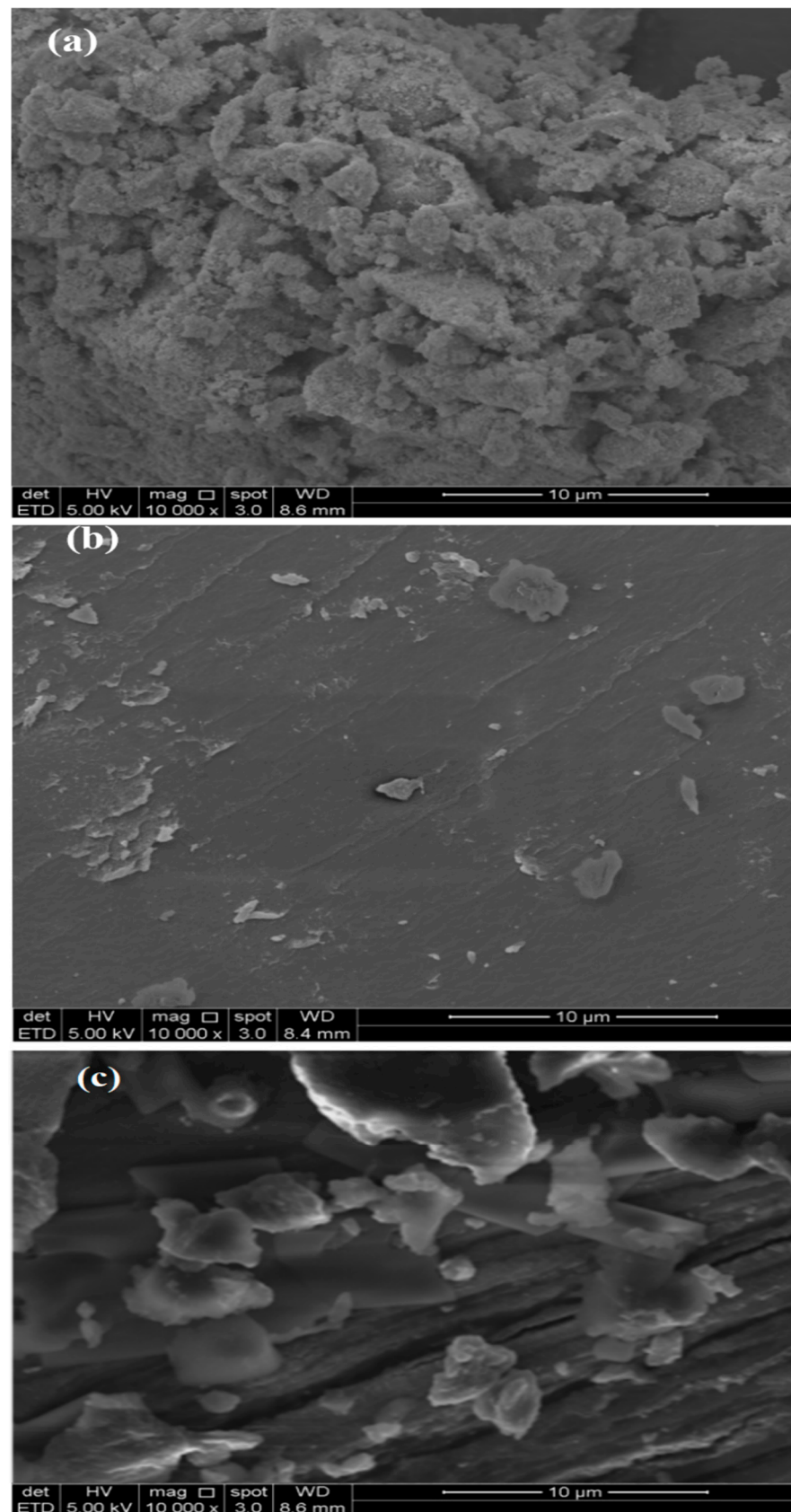


Figure 3. SEM images for (a)  $\text{Fe}_3\text{O}_4$ , (b) GA, and (c) GA-MNPs.

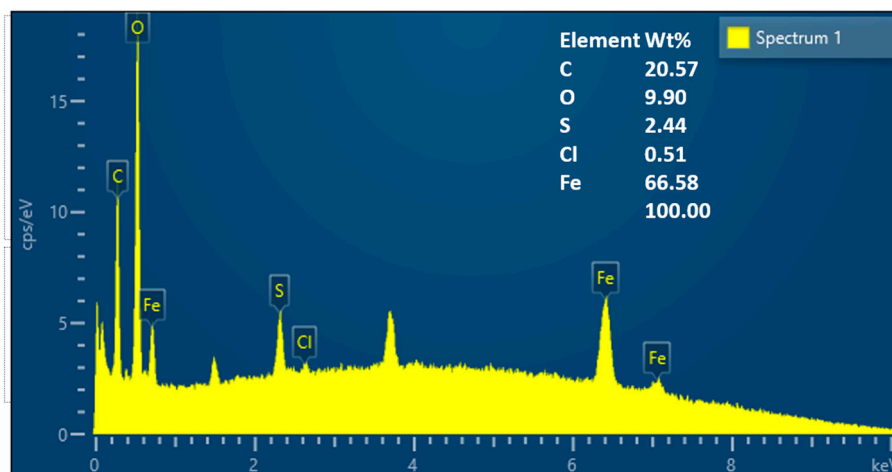


Figure 4. EDX analysis for GA-MNPs.

3.2. Effects of Interactive Variables during Process Optimization by RSM

The CCD-RSM was used to illustrate the experimental and anticipated adsorption capacity of GA-MNPs onto CIP. Following the design matrix shown in Table 3, the effects of optimizing and simultaneously interacting with the key adsorption parameters on the response were investigated. Equation (14) represents the quadratic model derived from the coded components.

Using the RSM model, the equation variables were signified as pH (A), CIP concentration (B), temperature (°C), GA-MNPs dose (D), and contact time (E).

$$\begin{aligned}
 \text{CIP adsorption capacity (mg/g)} = & + 92.08 + 0.2027A + 1.22B + 1.40C + \\
 & 0.6107D - 0.2113E + 0.0784AB + 0.4566AC - 0.9791AD + 0.8859AE - \\
 & 2.66BC + 0.0491BD - 0.6634BE + 0.6003CD - 1.54CE - 0.0184DE + \\
 & 0.3523A^2 - 2.44B^2 + 0.6586C^2 + 0.51361D^2 + 0.6461E^2
 \end{aligned}
 \tag{14}$$

The equation stated in accordance with coded factors allows one to predict the reaction for certain concentrations of each ingredient. The high levels of the components were by default expressed as +1 and the low levels as -1. The coded equation may be used to compare the factor coefficients and estimate the relative significance of the components.

Table 3. Design matrix for CIP removal.

Run	Factors					Contaminant Removal
	pH	CIP Concentration (ppm)	Temp. (°C)	GA-MNPs Dose (mg)	Contact Time (min)	CIP Removal (%)
1	10	60	45	30	72	95.24
2	6	60	45	30	72	90.51
3	8	40	35	40	96	91.73
4	4	40	55	20	48	96.04
5	6	60	45	10	72	94.43
6	8	80	35	40	48	93.57
7	6	60	45	30	72	92.18
8	4	40	35	20	48	81.42
9	8	40	35	20	96	80.65
10	6	60	45	30	120	97.14
11	4	40	35	20	96	82.29
12	6	60	45	30	72	96.74
13	4	80	35	20	48	92.01
14	2	60	45	30	72	93.23
15	4	40	35	40	96	97.54
16	4	80	35	20	96	95.93

**Table 3.** *Cont.*

Run	Factors					Contaminant Removal
	pH	CIP Concentration (ppm)	Temp. (°C)	GA-MNPs Dose (mg)	Contact Time (min)	CIP Removal (%)
17	6	60	45	30	72	95.07
18	6	60	45	30	24	93.68
19	6	60	45	30	72	82.92
20	6	60	45	30	72	82.15
21	6	60	45	30	72	98.64
22	6	20	45	30	72	83.79
23	8	40	55	20	96	97.84
24	4	80	55	20	48	93.11
25	8	80	55	40	48	94.33
26	4	80	55	40	48	98.64
27	4	80	35	40	48	97.03
28	8	80	35	20	96	96.17
29	6	60	65	30	72	94.78
30	8	40	35	20	48	84.02
31	4	40	55	40	96	83.25
32	4	40	55	40	48	99.74
33	4	40	35	40	48	84.89
34	6	60	25	30	72	96.14
35	8	80	55	40	96	91.41
36	8	80	35	40	96	92.63
37	6	60	45	30	72	96.94
38	6	60	45	50	72	95.33
39	4	40	55	20	96	94.47
40	8	80	55	20	96	93.08
41	6	100	45	30	72	82.32
42	8	40	35	40	48	81.55
43	8	40	55	20	48	98.04
44	4	80	55	20	96	83.19
45	4	80	55	40	96	94.54
46	4	80	35	40	96	89.81
47	8	80	55	20	48	91.03
48	8	80	35	20	48	95.34
49	8	40	55	40	96	93.73
50	8	40	55	40	48	92.87

### 3.2.1. Analysis of Variance (ANOVA)

The model significance was investigated by using the ANOVA presented in Table 4. The F-value of 1.44 for the model recommends that it is vital. Moreover, 18.34% of the time is noise capable of producing an F-value this high. When model terms have *p*-values under 0.0500, they are considered significant. In this case, the key model terms are BC and B2. If the value is more than 0.1000, the model terms are not important. According to the F-value for the lack of fit, which is 0.57, model reduction may be helpful if your model contains many unnecessary words (except those needed to maintain hierarchy). The lack of fit is not significant in comparison to the pure error. There is an 85.37% likelihood that noise is the root cause of a high Lack of Fit F-value. We seek a slight lack of fit because the model needs to be fit. Interactions between the optimal variables from the statistical ANOVA data are regarded as vital when the *p*-value is lower than 0.05. Thus, the most notable interactions are contact time and CIP concentration, GA-MNPs dose and pH, as well as CIP concentration and pH.

**Table 4.** ANOVA by RSM for CIP removal efficiencies.

Source	Sum of Squares	df	Mean Square	F-Value	p-Value	
Model	777.01	20	38.85	1.44	0.1834	significant
A-pH	1.64	1	1.64	0.0607	0.8071	
B-CIP concentration.	59.56	1	59.56	2.20	0.1488	
C-Temp.	78.43	1	78.43	2.90	0.0994	
D-GA-MNPs dose	14.92	1	14.92	0.5512	0.4638	
E-Contact time	1.79	1	1.79	0.0659	0.7992	
AB	0.1969	1	0.1969	0.0073	0.9326	
AC	6.67	1	6.67	0.2464	0.6234	
AD	30.67	1	30.67	1.13	0.2959	
AE	25.12	1	25.12	0.9278	0.3434	
BC	226.05	1	226.05	8.35	0.0072	
BD	0.0770	1	0.0770	0.0028	0.9578	
BE	14.08	1	14.08	0.5203	0.4765	
CD	11.53	1	11.53	0.4260	0.5191	
CE	75.68	1	75.68	2.80	0.1053	
DE	0.0109	1	0.0109	0.0004	0.9841	
A <sup>2</sup>	3.97	1	3.97	0.1467	0.7045	
B <sup>2</sup>	190.94	1	190.94	7.05	0.0127	
C <sup>2</sup>	13.88	1	13.88	0.5127	0.4797	
D <sup>2</sup>	8.44	1	8.44	0.3118	0.5809	
E <sup>2</sup>	13.36	1	13.36	0.4934	0.4880	
Residual	785.07	29	27.07			
Lack of Fit	503.05	22	22.87	0.5676	0.8537	not significant
Pure Error	282.02	7	40.29			
Cor Total	1562.08	49				

### 3.2.2. D Surface Plots

The contour and 3D surface plots in Figure 5a–f show the link between the independent variables, real and anticipated values of CIP adsorption capacity (mg/g). The effect of the interaction of CIP concentration and GA-MNPs dose is illustrated in Figure 5a,b. The quantity of adsorbent needed to reach the best adsorption capacity was 20 mg. The adsorption capacity did not change significantly with further adsorbent addition. This pattern suggested that CIP can be effectively removed by using a little amount during the adsorption process [53,55]. The common interaction between CIP concentration (20–100 ppm) and contact time (24 to 120 min) is shown in Figure 5c,d with all other parameters being held at their optimal values. The effectiveness of CIP adsorption rose with contact time and diminished with an increase in CIP concentration [55]. This is because all the CIP molecules were readily bonded to the GA-MNPs active sites at lower doses [56]. Because the GA-MNPs are porous in nature and have both active and unoccupied adsorption sites, quick equilibration was accomplished with only 24 min of contact time. The adsorption equilibration time is reached in 48 min and remains unchanged for the remaining 72 min [57]. To comprehend the surface charge of the adsorbent and the degree of ionization of the adsorbate molecule, the effect of pH variations ranging from 2 to 10 as illustrated in Figure 5e,f was investigated. The aqueous solution was switched to the anionic form at low pH values (2 to 6), becoming negatively charged because of deprotonation and producing a positively charged GA-MNPs

surface. At pH 4, the aqueous solution had a negative charge whereas the surface of the adsorbent had a positive charge. Due to the potential for electrostatic contact, there is a large increase in the capacity for adsorption [54,58]. The deprotonated surface charge of the adsorbent and molecule at high pH changed the chances of electrostatic contact. As a result, the electrostatic repulsion caused the adsorption capacity to diminish. This could be based on the CIP molecules and -OH intense battle for active empty sites [59]. Additionally, higher pH levels caused several functional groups, such as carbonyl and hydroxyl, to be in their protonated cationic form which slows down effective adsorption [60]. Thus, the greatest adsorption conditions are described as contact time 48 min, CIP concentration 60 ppm, 20 g GA-MNPs dosage, pH 6, and temperature 35 °C.

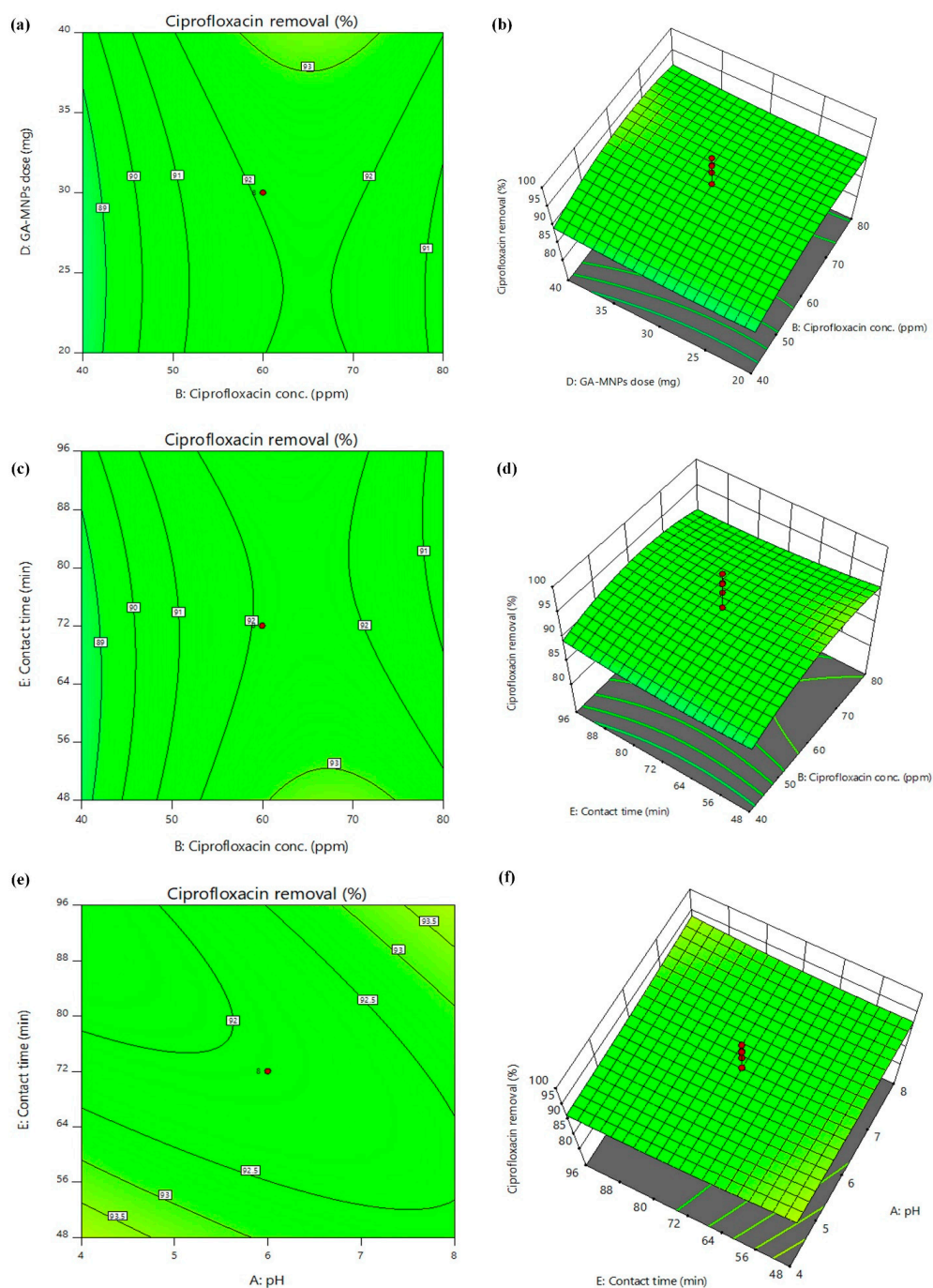


**Figure 5.** Contour plots and 3D response surface plots of CIP removal reveal the interactive effects of (a,b) CIP conc. and GA-MNPs dose, (c,d) CIP conc. and contact time, (e,f) pH, and contact time.

### 3.2.3. Normal and Predicted Plots

Figure 6 depicts the link between actual and predicted values. The experimental and predicted response values have a favorable association. Figure 7 demonstrates the association between externally studentized residuals and CIP removal. It also demonstrates a strong link between the variables.

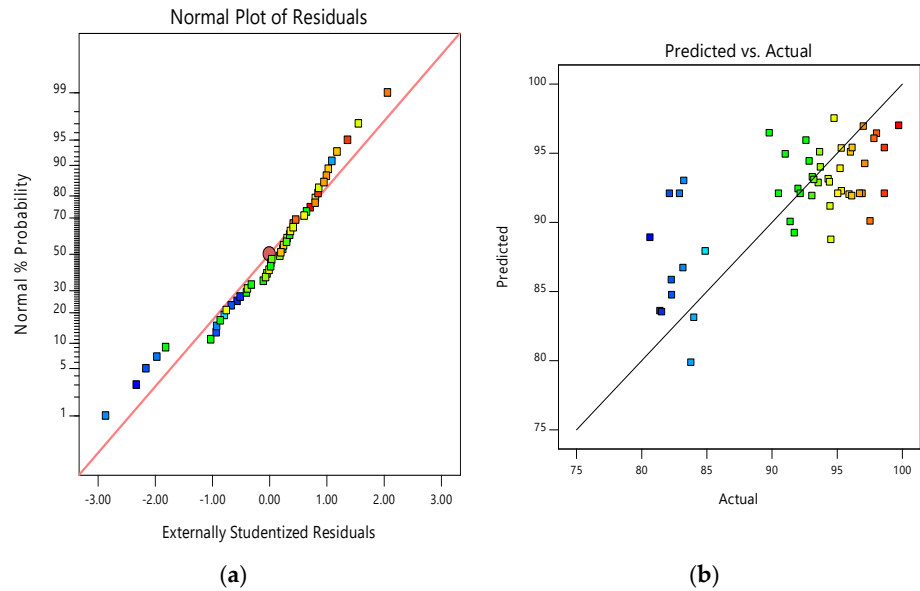


**Figure 6.** Design-expert plots of (a) normal probability curve of the residuals and (b) relationship between actual values and predicted values for CIP removal.

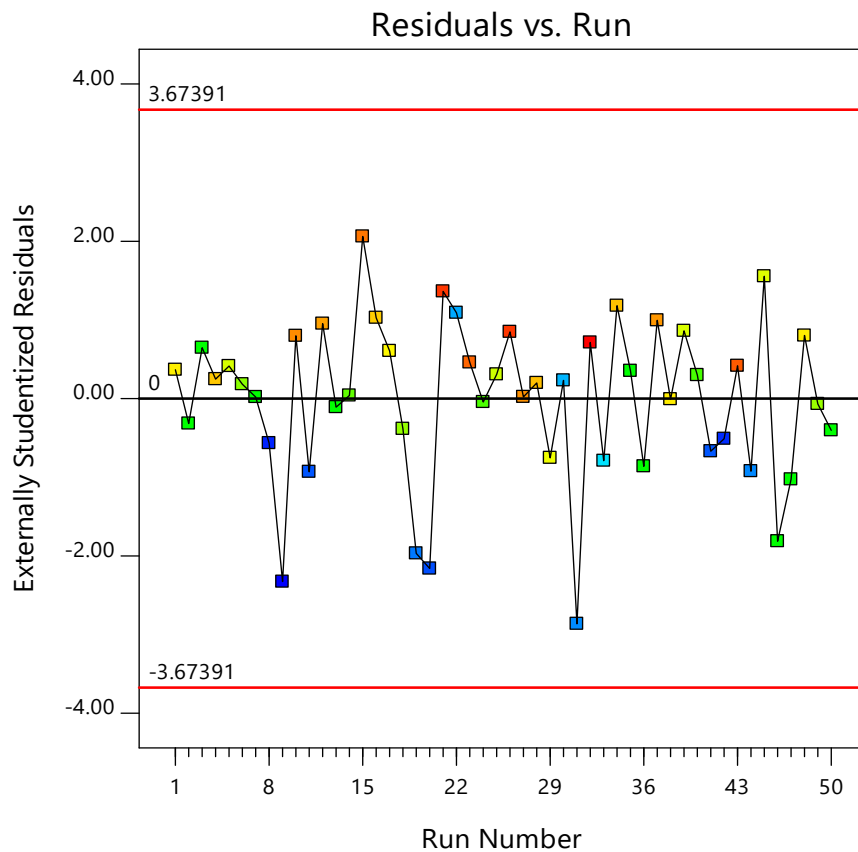


**Figure 7.** Probability plot of externally studentized residuals vs. Run Number for CIP removal.

The CCD-RSM multiple regression analysis yielded a substantial prediction, with values acquired during the model comparison and fit statistics shown in Table 5. The model confidence level was set at 95%. This demonstrates a strong relationship between  $R^2$  and Adjusted  $R^2$ . According to a low Predicted  $R^2$ , the mean might be a more interesting predictor of your reaction than the present model. In certain cases, a higher order model may also provide more accurate predictions. The signal-to-noise ratio is defined by Adeq Precision. The ideal ratio is larger than 4. According to the signal-to-noise ratio of 5.2332, the signal seems satisfactory. Thus, this model is useful for navigating the design space.

**Table 5.** Model comparison and fit statistics for CIP removal.

Model Comparison Statistics		Fit Statistics	
PRESS	2165.67	Std. Dev.	5.20
−2 Log Likelihood	279.58	Mean	91.86
BIC	361.73	C.V. %	5.66
AICc	354.58	$R^2$	0.4974
		Adjusted $R^2$	0.1508
		Predicted $R^2$	−0.3864
		Adeq Precision	5.2332

Assuming that all other variables remain the same, the coefficient estimates in terms of coded factors provided in Table 6 indicate the expected change in response for each unit change in the factor value. The average reaction of overall runs in an orthogonal design are the intercept. The coefficients alter the factor settings produced around that average. When the factors are orthogonal, VIFs are 1, VIFs exceed 1, and the severity of the factor correlation rises with rising VIF values. VIFs under 10 are often acceptable.

**Table 6.** Coefficients in terms of coded factors for the responses (CIP removal).

	Coefficient Estimate	df	Standard Error	95% CI Low	95% CI High	VIF
Intercept	92.08	1	1.80	88.39	95.77	
A2212 pH	0.2027	1	0.8227	2212 1.48	1.89	1.0000
B2212 CIP concentration	1.22	1	0.8227	2212 0.4623	2.90	1.0000
C2212 Temp.	1.40	1	0.8227	2212 0.2823	3.08	1.0000
D2212 GA2212 MNPs dose	0.6107	1	0.8227	2212 1.07	2.29	1.0000
E2212 Contact time	−0.2113	1	0.8227	−1.89	1.47	1.0000
AB	0.0784	1	0.9198	−1.80	1.96	1.0000
AC	0.4566	1	0.9198	−1.42	2.34	1.0000
AD	−0.9791	1	0.9198	−2.86	0.9021	1.0000
AE	0.8859	1	0.9198	−0.9952	2.77	1.0000
BC	−2.66	1	0.9198	−4.54	−0.7767	1.0000
BD	0.0491	1	0.9198	−1.83	1.93	1.0000
BE	−0.6634	1	0.9198	−2.54	1.22	1.0000
CD	−0.6003	1	0.9198	−2.48	1.28	1.0000
CE	−1.54	1	0.9198	−3.42	0.3433	1.0000
DE	−0.0184	1	0.9198	−1.90	1.86	1.0000
A <sup>2</sup>	0.3523	1	0.9198	−1.53	2.23	1.0000

Table 6. Cont.

	Coefficient Estimate	df	Standard Error	95% CI Low	95% CI High	VIF
B <sup>2</sup>	−2.44	1	0.9198	−4.32	−0.5615	1.0000
C <sup>2</sup>	0.6586	1	0.9198	−1.22	2.54	1.0000
D <sup>2</sup>	0.5136	1	0.9198	−1.37	2.39	1.0000
E <sup>2</sup>	0.6461	1	0.9198	−1.24	2.53	1.0000

3.3. Sorption Kinetics

The adsorption kinetic models are used to study adsorbents’ interaction with adsorbates [61]. Adsorption efficiency is the primary factor used to measure absorption efficiency and is defined as a change in adsorption per unit of time [62]. Figure 8a–d depicts the linear fitting results for pseudo–first order, pseudo-second order, elovich, and intraparticle diffusion for the sorption rate of CIP on GA-MNPs. The kinetic parameters that correspond with the correlation coefficients of kinetic models are described in Table 7. The sorption mode is shown to be better described by pseudo-second order model in comparison to pseudo-first order model with R<sup>2</sup> values 0.9984. This suggests chemisorption adsorption processes as the q<sub>e cal</sub> of the model was nearer to the experimental value q<sub>e exp</sub> [54,63].

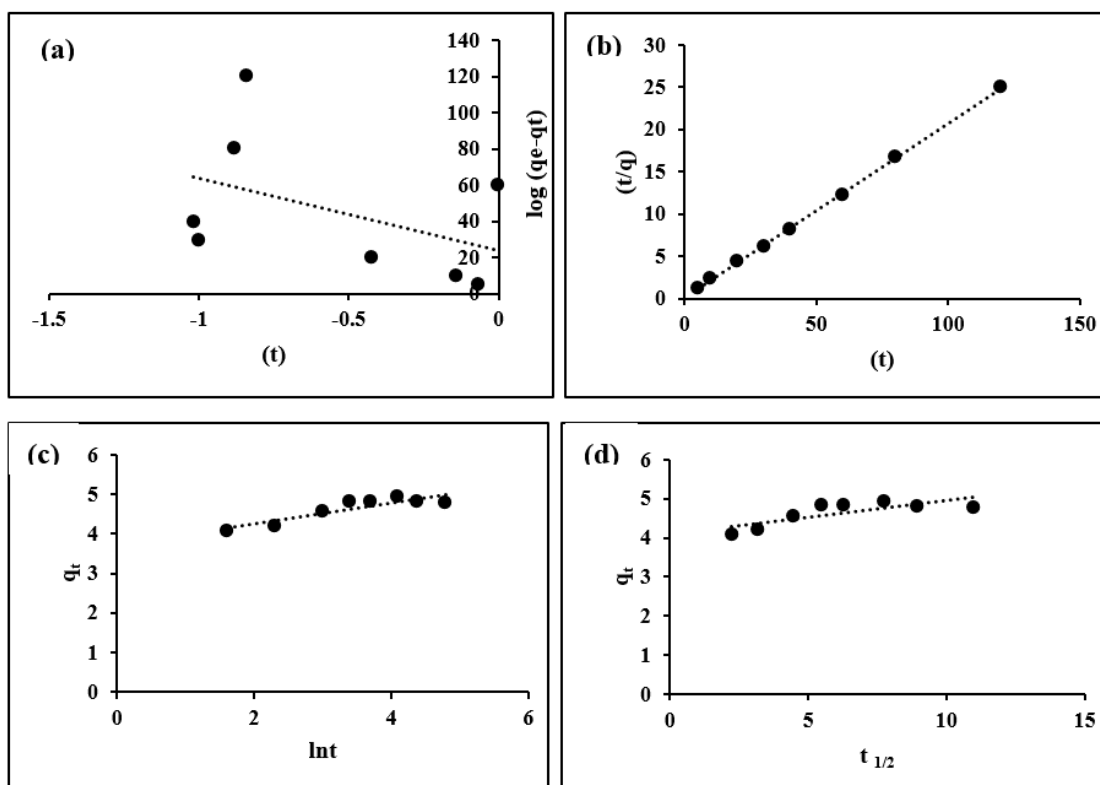


Figure 8. (a) pseudo-first order, (b) pseudo-second order, (c) Elovich, and (d) Intraparticle diffusion kinetic models for the adsorption of CIP on GA-MNPs.

Table 7. Kinetic models for the CIP removal by GA-MNPs.

	Pseudo-First-Order	Pseudo-Second-Order	Elovich	Intraparticle Diffusion			
q <sub>e exp</sub>	4.929	q <sub>e cal</sub>	4.8473	q <sub>e cal</sub>	19.6405		
q <sub>e cal</sub>	1.3799	K <sub>2</sub>	0.3118	β	3.7693	C	4.1065
K <sub>1</sub>	91.0905	h	7.3266	α	0.7007	K	0.0844
R <sup>2</sup>	0.1936	R <sup>2</sup>	0.9984	R <sup>2</sup>	0.7939	R <sup>2</sup>	0.6099

### 3.4. Adsorption Isotherm

The effective adsorption properties between adsorbent and adsorbate are explained using sorption isotherms, which are defined by certain constants values that reflect the properties of the adsorbent surface and the equilibrium affinity of the sorbent sorption [64]. Figure 9. demonstrates the linear plots of Langmuir, Freundlich, Temkin, and Dubinin–Radushkevich isotherm models. Table 8 shows the important parameters that were determined using the isotherm model’s linear plots. The maximum adsorption capacity value ( $q_{max}$ ) was derived from a plot of the Langmuir ( $54.6449 \text{ mg g}^{-1}$ ), The Freundlich isotherm model fits the experimental findings with  $R^2$  value (0.9836). The Freundlich isotherm model characterizes that the adsorption method occurred on heterogeneous surfaces [65]. Furthermore, the constants  $n$  for the Freundlich model were larger than 1, indicating the favorability of adsorption [66].

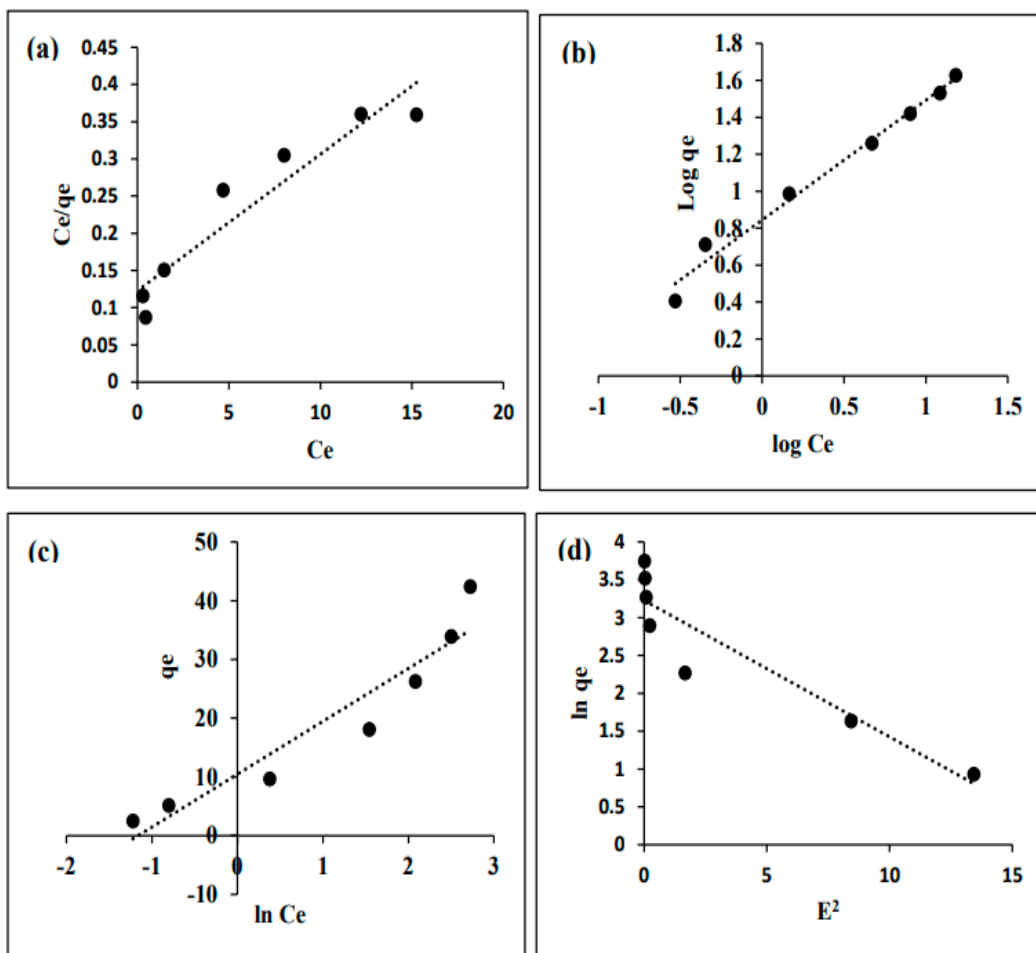


Figure 9. (a) Langmuir, (b) Freundlich, (c) Temkin, and (d) D-R isotherm models for the adsorption of CIP on GA-MNPs.

Table 8. Isotherm models for the adsorption of CIP using GA-MNPs.

	Langmuir	Freundlich	Temkin	Dubinin–Radushkevich
$q_{max}$	54.6449	$K_F$	6.982	$K_T$ 3.196
$R_L$	0.1007	$n_F$	1.542	$b$ 275.24
$R^2$	0.9026	$R^2$	0.9836	$R^2$ 0.9025
				$q_{max}$ 25.2065
				$E$ 4.7114
				$R^2$ 0.8613

### 3.5. Thermodynamics Studies

Table 9 summarizes the thermodynamic parameters obtained from the Van't-Hoff plot as can be seen in Figure 10. The negative  $\Delta G^\circ$  values showed that CIP adsorption on the GA-MNPs was a spontaneous process. When the absolute value of  $\Delta G^\circ$  was between 80 and 200 KJ mol<sup>-1</sup>, the adsorption might be attributed to chemical adsorption, while those between 2.1–20.9 KJ mol<sup>-1</sup> suggests physical adsorption present. Lower negative  $\Delta G^\circ$  values with higher temperatures indicate that CIP adsorption was thermodynamically more advantageous in lower temperature [51]. Therefore, CIP adsorption on GA-MNPs might be explained as physical adsorption enabled by the electrostatic effect. The exothermic nature of the adsorption with a negative value of  $\Delta H$  (−40 KJ/mol), aligns with the physical adsorption. The negative value of  $\Delta S$  exhibited that the randomness of CIP adsorption was lowered [5,67].

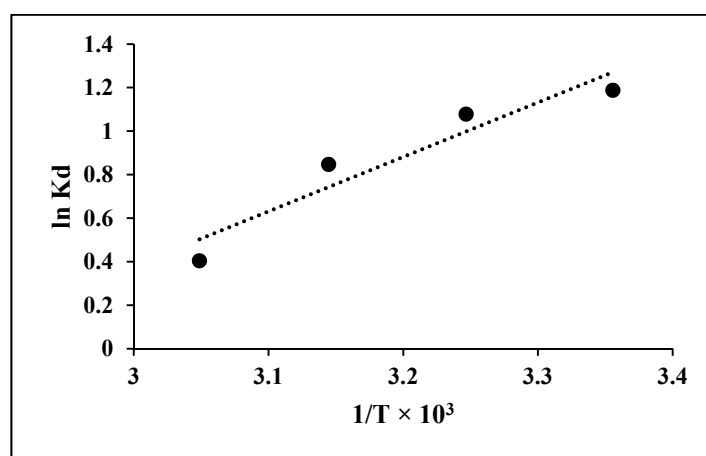


Figure 10. Van't-Hoff's plot for adsorption of ENR using GA-MNPs.

Table 9. Thermodynamic parameters for the adsorption of CIP GA-MNPs.

T (K)	Enthalpy, $\Delta H$ (kJ mol <sup>-1</sup> )	Entropy, $\Delta S$ (J mol <sup>-1</sup> K <sup>-1</sup> )	Gibbs Energy, $\Delta G$ (kJ mol <sup>-1</sup> )
298			−2945.0376
308			−2764.2747
318	−20.79	−59.21	−2241.324
328			−1102.7939

### 3.6. Adsorption Mechanism

Figure 11 showed the proposed mechanism for the adsorption of CIP on GA-MNPs. The anticipated interactions present are electrostatic interaction,  $\pi$ - $\pi$  stacking, and hydrogen bonding. Numerous functional groups such as -NH, -OH, and -COOH were widely present on the surface of GA-MNPs and CIP. Moreover, CIP also contains benzene, and F-based groups, which can be involved in the adsorption process between CIP and GA-MNPs [4].

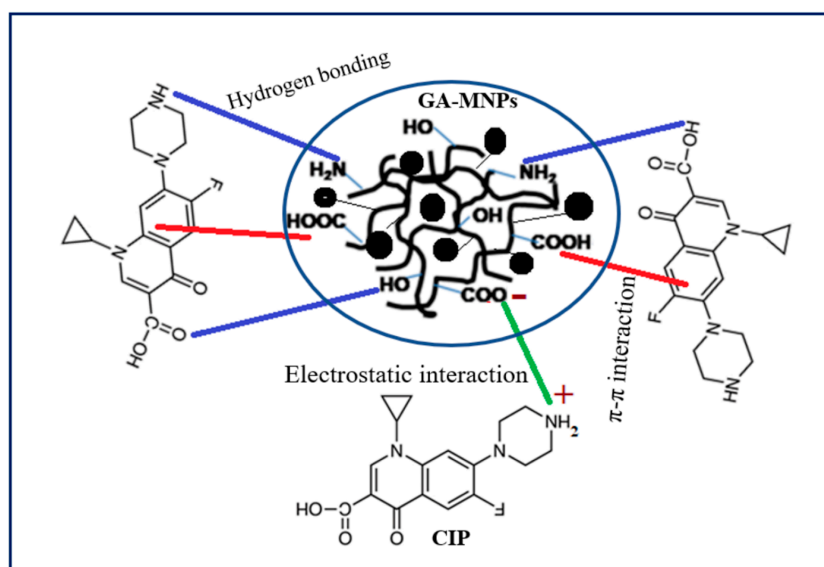


Figure 11. Mechanism for CIP adsorption onto the GA-MNPs.

### 3.7. Comparison of the GA-MNPs with Other Reported Adsorbents

The maximum adsorption capacity  $q_{max}$  achieved in this study was compared with those reported in literature as shown in Table 10. This is to assess the CIP adsorption efficiency of the GA-MNPs. Based on the findings, the  $q_{max}$  value of the current study is better than other reported adsorbents such as magnesium oxide nanoparticles, halloysite nanotubes, schorl, and activated carbon. GA-MNPs were also able to remove the CIP in a short time. Therefore GA-MNPs could be used as a sorbent’s alternative for the CIP contaminants removal from aqueous solutions.

Table 10. Comparison of reported adsorbents with GA-MNP used for CIP removal.

Adsorbent	pH	Isotherm Models	Kinetic Models	Percentage Removal (%R)	$q_e$ (mg g <sup>-1</sup> )	Equilibrium Time	Ref
Schorl	5.5	Freundlich	pseudo-second-order	-	8.49	720 min	[66]
Magnesium Oxide Nanoparticles	5.7	Langmuir	pseudo-second-order	85	3.46	60 min	[68]
Oat hulls	7	Freundlich	pseudo-second-order	-	83	-	[51]
Aluminum-Pillared Kaolin	4	Langmuir	pseudo-first-order	-	68.36	1440 min	[67]
Sodium Alginate Beads	7	-	pseudo-first-order	96	-	80 min	[69]
Nanocomposite/membrane	-	Freundlich	pseudo-first-order	91.84	1.7446	120 min	[25]
Multiwall carbon nanotube	-	Freundlich and Langmuir	pseudo-first-order	-	72	1440 min	[11]
Birnessite	6	Freundlich	pseudo-second-order	-	-	1440 min	[70]
Biochar	8	Freundlich	pseudo-second-order	-	-	1440 min	[70]
Activated carbon	-	Freundlich	pseudo-second-order	93.39	0.4680	200 min	[26]
Wheat bran	3	Langmuir and D-R	pseudo-second-order	-	159	60 min	[71]
Halloysite Nanotubes	6	Langmuir	pseudo-second-order	-	1.0172	90 min	[72]
GA-MNPs	7	Freundlich	pseudo-second-order	96.34	54.6449	60 min	This study

### 3.8. Adsorbent Regeneration and Reusability

To reduce the cost of the adsorption process, reusability of an adsorbent material is an ultimately important parameter to be considered for practical and commercial application of the material in real samples [73]. Thus, a good adsorbent material should be easily regenerated and reused. Acid and alkali treatment helps the recoverability and regeneration of the adsorbents. However, it could damage the body of the adsorbent resulting in a decrease in its adsorption capacity after each regeneration cycle. Thus, the choice of good acid/alkali and their concentration becomes paramount.

In this work, the percentage removals of CIP were determined at seven (7) successive cycles. After the adsorption of CIP, the adsorbed and saturated GA-MNPs was dispersed in a 40% methanol solution, agitated for 6 h at room temperature, and washed three times. Subsequently, the regenerated GA-MNPs was again used to absorb CIP. The desorbed samples were then collected using the suction filtering technique and rinsed with distilled water. To reuse the samples in the next round of adsorption studies, they were finally dried in an oven at 70 °C. Figure 12 shows the effect of the number of regeneration cycles on the CIP adsorption capacity of GA-MNPs. High removal percentage was maintained by the adsorbent until the third cycle (91.73%). Subsequent removal trials in the fourth, fifth, sixth, and seventh cycles showed a slight decline in the adsorption of CIP by (5.74, 7.53, 10.26, and 12.41%), respectively. This can be due to the loss of a slight amount of adsorbent during the recycling process. Despite the slight reduction in the removal of CIP, the GA-MNPs still retained >80% removal efficiency after the seventh cycle.

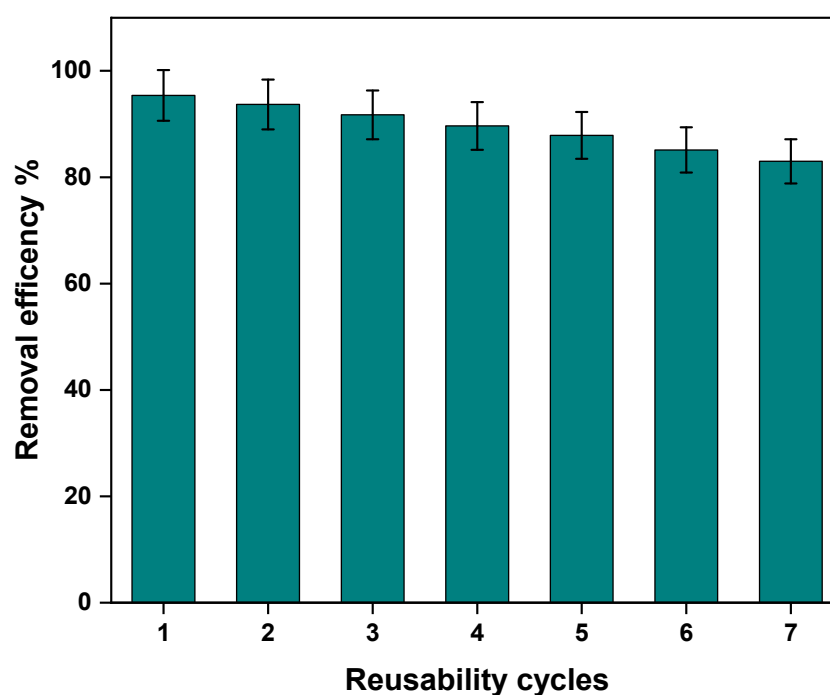


Figure 12. Reusability of the GA-MNPs for the removal of CIP.

Interestingly, after the GA-MNPs chelator was subjected to seven (7) sorption-regeneration cycles, the adsorption capacity was still 82.99% of the initial capacity which shows the excellent life cycle of the developed adsorbent. The changes in mass before and after adsorption was observed to be negligible, especially in the last three cycles. Findings also showed a trivial increase in adsorbent capacity loss with a decrease in adsorptive efficiency after seven adsorption/desorption cycles as evidenced by Figure 11. This observation can be attributed to the fact that there is a decrease in active sites of GA-MNPs. The decline in efficiency is less than 3% which indicates that the GA-MNPs has a high recyclability and nearly maintains a constant regeneration efficiency after 7 cycles. Consequently,

the result implied that GA-MNPs could be successfully regenerated. Thus, the stability of the GA-MNPs in relation to the effective removals of the pollutants after considerable number of repeated uses could be employed as a measure of their potentiality as effective and economical adsorbing material for removing CIP from contaminated solution.

The results of this study are comparable to many reported studies on the regeneration of adsorbents as highlighted in Table 11 below. The adsorbent developed by Sharma et al. [4] demonstrated 67% of its initial adsorption capacity after six sorption regeneration cycles. Duran et al. [74], on the other hand, estimated a 10% capacity loss after four sorption-regeneration cycles. Baloo et al. [75] estimated that their two adsorbents showed 27.21 and 60.11% of their initial adsorption capacity after five sorption-regeneration cycles. In another study, the modified resin by Afolabi et al. [76] showed 77.2% of its original capacity after five cycles. This demonstrates the effectiveness and reusability of our developed adsorbent.

**Table 11.** Comparison for different adsorbents on regeneration cycles.

Contaminant	Adsorbent	No. of Re-generation Cycles	Maximum Adsorption Capacity (mg/g)	Initial Removal Efficiency	Final Removal Efficiency	% Loss	Ref.
Boron	Poly saccharide derivative functional hollow silica sphere (HSGUM)	4	217.4	88	63	25	[74]
Pb(II)	Fe3O4@TATS@ATA Gum	4	205.2	91	78	13	[14]
Crystal violet dye.	arabic-cl-poly(acrylamide) nanohydrogel	6	90.90	79	67	12	[4]
Pb(II)	UiO-66-NH <sub>2</sub> modified by Glycidyl methacrylate (GMA)	5	238.80	84	80.53	3.47	[73]
Cd(II)			208.45	90	83.67	6.33	
Boron	Polymeric chelator containing glycidol moiety	5	25.7	98.94	95.21	3.73	[23]
Methylene blue dyes	Oil palm wastes-derived activated carbon	5	54.00	98.09	72.21	25.88	[75]
Acid orange 10 dyes			36.75	78.58	60.11	18.47	
CIP	GA-MNPs	7	54.64	96.34	82.99	13.35	This study

#### 4. Conclusions

The study synthesized and subsequently utilized GA-MNPs for the adsorption of CIP. The GA-MNPs was characterized by FTIR, SEM, and EDX analysis to determine its morphology and physicochemical properties. Optimization by RSM based on CCD was conducted to determine the optimum conditions for the most efficient adsorption capacity through the simultaneous interaction of adsorption parameters using 50 runs. R<sup>2</sup> 0.9409 showed that the model was relevant for CIP removal. Model terms are symbolic, as shown by the model’s F-value of 1.44 and low probability value (Prob. > F 0.0001). Different initial concentrations were varied against time to study the adsorption kinetics. Findings revealed that the kinetic results followed the pseudo-second order model that indicated high adsorption capacity of 54.6449 mg/g was achieved at a contact time of 48 min, CIP concentration 60 ppm, 20 g GA-MNPs dosage, pH 6, and temperature 35 °C. The isotherm fit best with the Freudlinch multilayer model, and the adsorption displays a spontaneous process and exothermic nature for the calculated thermodynamic parameters with increased randomness at the liquid–solid interface. This suggests double-layer adsorption and designate that a heterogeneous surface was obtained for the adsorption of CIP on GA-MNPs. The GA-MNPs adsorbent achieved 96.30% CIP removal from aqueous solution.

The interaction and binding mechanism showed the presence of hydrogen bonding, electrostatic interaction and  $\pi$ - $\pi$  interaction between the GA-MNPs and CIP. The reusability of the adsorbent was studied for seven adsorption–desorption cycles and the GA-MNPs displayed good reusability performance with a slight decline from 96.45% to 82.99% occurring after seven repeated experimental cycles. The ease of regeneration makes them suitable for repeated and large-scale applications with effective performance in terms of CIP removal. Comparison with other previously reported adsorbents showed the superiority potential of GA-MNPs in terms of surface area, adsorption capacity, equilibration time, regeneration capability, and impact during environmental clean-up. GA-MNPs is an outstanding adsorbent for efficient application in CIP removal from contaminated effluents. Thus, it can be concluded that the cost of GA-MNPs production is viable for commercial production. Future studies should intensify research efforts by investigating the use of GA-MNPs with other pharmaceutical active compounds and pesticide residue in a different matrix such as food and beverage. More so, the commercial exploitation of this adsorbent must focus on production routes that are cost-effective in the synthesis procedure.

**Author Contributions:** Conceptualization, Methodology, A.H.B., R.E.A.M., S.S.A. and A.H.J.; writing-original draft preparation, A.H.B., R.E.A.M., S.S.A. and A.H.J.; visualization, A.H.B., R.E.A.M., S.S.A. and A.H.J.; investigation, A.H.B., R.E.A.M., S.S.A. and A.H.J.; material synthesis and characterizations, A.H.B., R.E.A.M., A.H.J. and S.S.A.; results interpretation, A.H.B., R.E.A.M., S.S.A., M.F.R. and A.H.J.; writing reviewing and editing, A.H.B., R.E.A.M., S.S.A., A.H.J., S.M. and A.C.S.; supervision and funding acquisition, M.F.R., S.M.E. and M.A. All authors have read and agreed to the published version of the manuscript.

**Funding:** This research received no external funding.

**Data Availability Statement:** The data can be found within the manuscript.

**Acknowledgments:** The authors wish to acknowledge the grants received from Tertiary Education Trust Fund (TETFUND) Nigeria.

**Conflicts of Interest:** Authors declare no conflicts of interest.

## References

1. Almeida, C.M. Overview of Sample Preparation and Chromatographic Methods to Analysis Pharmaceutical Active Compounds in Waters Matrices. *Separations* **2021**, *8*, 16. [[CrossRef](#)]
2. Anucha, C.B.; Altin, I.; Bacaksız, E.; Kucukomeroglu, T.; Belay, M.H.; Stathopoulos, V.N. Enhanced photocatalytic activity of CuWO<sub>4</sub> doped TiO<sub>2</sub> photocatalyst towards carbamazepine removal under UV irradiation. *Separations* **2021**, *8*, 25. [[CrossRef](#)]
3. Abdullahi, S.S.A.; Musa, H.; Habibu, S.; Birniwa, A.H.; Mohammad, R.E.A. Facile synthesis and dyeing performance of some disperse monomeric and polymeric dyes on nylon and polyester fabrics. *Bull. Chem. Soc. Ethiop.* **2021**, *35*, 485–497. [[CrossRef](#)]
4. Sharma, G.; Kumar, A.; Naushad, M.; García-Peñas, A.; Ala'á, H.; Ghfar, A.A.; Sharma, V.; Ahamad, T.; Stadler, F.J. Fabrication and characterization of Gum arabic-cl-poly (acrylamide) nanohydrogel for effective adsorption of crystal violet dye. *Carbohydr. Polym.* **2018**, *202*, 444–453. [[CrossRef](#)]
5. Trovato, E.; Arigò, A.; Vento, F.; Micalizzi, G.; Dugo, P.; Mondello, L. Influence of citrus flavor addition in brewing process: Characterization of the volatile and non-volatile profile to prevent frauds and adulterations. *Separations* **2021**, *8*, 18. [[CrossRef](#)]
6. Abdullahi, S.S.; Birniwa, A.H.; Chadi, A.S.; Mohammad, R.E.A.; Mamman, S. Effect of Fiber Surface Modification on the Mechanical Properties of Rice Husk/Glass Fiber Reinforcement Epoxy Resin Hybrid Composite. *Niger. Res. J. Chem. Sci.* **2020**, *8*, 147–162.
7. Fadzli, F.S.; Bhawani, S.A.; Mohammad, R.E. Microbial fuel cell: Recent developments in organic substrate use and bacterial electrode interaction. *J. Chem.* **2020**, *2021*, 4570388. [[CrossRef](#)]
8. Jagaba, A.H.; Kutty, S.R.M.; Abubakar, S.; Birniwa, A.H.; Lawal, I.M.; Umaru, I.; Usman, A.K.; Yaro, N.S.A.; Al-Zaqri, N.; Al-Maswari, B.M.; et al. Synthesis, Characterization, and Performance Evaluation of Hybrid Waste Sludge Biochar for COD and Color Removal from Agro-Industrial Effluent. *Separations* **2022**, *9*, 258. [[CrossRef](#)]
9. Abbasi, A.; Yahya, W.Z.N.; Nasef, M.M.; Moniruzzaman, M.; Ghumman, A.S.M.; Afolabi, H.K. Boron removal by glucamine-functionalized inverse vulcanized sulfur polymer. *React. Funct. Polym.* **2022**, *177*, 105311. [[CrossRef](#)]
10. Birniwa, A.H.; Abubakar, A.S.; Huq, A.O.; Mahmud, H.N.M.E. Polypyrrole-polyethyleneimine (PPy-PEI) nanocomposite: An effective adsorbent for nickel ion adsorption from aqueous solution. *J. Macromol. Sci. Part A Pure Appl. Chem.* **2021**, *58*, 206–217. [[CrossRef](#)]

11. Jiang, W.T.; Chang, P.H.; Wang, Y.S.; Tsai, Y.; Jean, J.S.; Li, Z.; Krukowski, K. Removal of ciprofloxacin from water by birnessite. *J. Hazard. Mater.* **2013**, *250*, 362–369. [[CrossRef](#)]
12. Jagaba, A.H.; Kutty, S.R.M.; Isa, M.H.; Ghaleb, A.A.S.; Lawal, I.M.; Usman, A.K.; Birniwa, A.H.; Noor, A.; Abubakar, S.; Umaru, I.; et al. Toxic Effects of Xenobiotic Compounds on the Microbial Community of Activated Sludge. *ChemBioEng Rev.* **2022**, *9*, 1–40. [[CrossRef](#)]
13. Abdullahi, S.S.; Musa, H.; Habibu, S.; Birniwa, A.H.; Mohammad, R.E.A. Comparative study and dyeing performance of as-synthesized azo heterocyclic monomeric, polymeric, and commercial disperse dyes. *Turk. J. Chem.* **2022**, *46*, 1–12.
14. Alqadami, A.A.; Naushad, M.; AlOthman, Z.A.; Alsuhybani, M.; Algamdi, M. Excellent adsorptive performance of a new nanocomposite for removal of toxic Pb (II) from aqueous environment: Adsorption mechanism and modeling analysis. *J. Hazard. Mater.* **2020**, *389*, 121896. [[CrossRef](#)]
15. Hong, H.J.; Kim, J.; Kim, D.Y.; Kang, I.; Kang, H.K.; Ryu, B.G. Synthesis of carboxymethylated nanocellulose fabricated ciprofloxacin–montmorillonite composite for sustained delivery of antibiotics. *Int. J. Pharm.* **2019**, *567*, 118502. [[CrossRef](#)]
16. Birniwa, A.H.; Abubakar, A.S.; Mahmud, H.N.M.E.; Kutty, S.R.M.; Jagaba, A.H.; Abdullahi, S.S.A.; Zango, Z.U. Application of agricultural wastes for cationic dyes removal from wastewater. In *Textile Wastewater Treatment*; Springer: Berlin/Heidelberg, Germany, 2022; pp. 239–274.
17. Jagaba, A.H.; Kutty, S.R.M.; Lawal, I.M.; Aminu, N.; Noor, A.; Al-dhawi, B.N.S.; Usman, A.K.; Batari, A.; Abubakar, S.; Birniwa, A.H.; et al. Diverse sustainable materials for the treatment of petroleum sludge and remediation of contaminated sites: A review. *Clean. Waste Syst.* **2022**, *2*, 100010. [[CrossRef](#)]
18. Wu, Q.; Que, Z.; Li, Z.; Chen, S.; Zhang, W.; Yin, K.; Hong, H. Photodegradation of ciprofloxacin adsorbed in the intracrystalline space of montmorillonite. *J. Hazard. Mater.* **2018**, *359*, 414–420. [[CrossRef](#)]
19. Jagaba, A.H.; Kutty, S.R.M.; Noor, A.; Affam, A.C.; Ghfar, A.A.; Usman, A.K.; Lawal, I.M.; Birniwa, A.H.; Kankia, M.U.; Afolabi, H.K. Parametric optimization and kinetic modelling for organic matter removal from agro-waste derived paper packaging biorefinery wastewater. *Biomass Convers. Biorefinery* **2022**, *2022*, 1–18. [[CrossRef](#)]
20. Gupta, A.; Garg, A. Degradation of ciprofloxacin using Fenton’s oxidation: Effect of operating parameters, identification of oxidized by-products and toxicity assessment. *Chemosphere* **2018**, *193*, 1181–1188. [[CrossRef](#)]
21. Peng, X.; Hu, F.; Lam, F.L.; Wang, Y.; Liu, Z.; Dai, H. Adsorption behavior and mechanisms of ciprofloxacin from aqueous solution by ordered mesoporous carbon and bamboo-based carbon. *J. Colloid Interface Sci.* **2015**, *460*, 349–360. [[CrossRef](#)]
22. Noor, A.; Kutty, S.R.M.; Jagaba, A.H.; Yusuf, M.; Akram, M.W.; Adil, M.R.; Ahmad, N.; Jamal, M. Kinetic modelling of nutrient removal of petroleum industry wastewater remediation. In Proceedings of the 2021 Third International Sustainability and Resilience Conference: Climate Change, Virtual Event, 15–16 November 2021; IEEE: New York, NY, USA, 2021; pp. 216–220.
23. Afolabi, H.K.; Nasef, M.M.; Nordin, N.A.H.M.; Ting, T.M.; Harun, N.Y.; Saeed, A.A.H. Isotherms, kinetics, and thermodynamics of boron adsorption on fibrous polymeric chelator containing glycidol moiety optimized with response surface method. *Arab. J. Chem.* **2021**, *14*, 103453. [[CrossRef](#)]
24. Naushad, M.; Ahamad, T.; Sharma, G.; Ala’a, H.; Albadarin, A.B.; Alam, M.M.; AlOthman, Z.A.; Alshehri, S.M.; Ghfar, A.A. Synthesis and characterization of a new starch/SnO<sub>2</sub> nanocomposite for efficient adsorption of toxic Hg<sup>2+</sup> metal ion. *Chem. Eng. J.* **2016**, *300*, 306–316. [[CrossRef](#)]
25. Avci, A.; İnci, İ.; Baylan, N. Adsorption of ciprofloxacin hydrochloride on multiwall carbon nanotube. *J. Mol. Struct.* **2020**, *1206*, 127711. [[CrossRef](#)]
26. Avci, A.; İnci, İ.; Baylan, N.A. Comparative adsorption study with various adsorbents for the removal of ciprofloxacin hydrochloride from water. *Water. Air. Soil Pollut.* **2019**, *230*, 1–9. [[CrossRef](#)]
27. Ahamad, T.; Naushad, M.; Al-Shahrani, T.; Al-Hokbany, N.; Alshehri, S.M. Preparation of chitosan based magnetic nanocomposite for tetracycline adsorption: Kinetic and thermodynamic studies. *Int. J. Biol. Macromol.* **2020**, *147*, 258–267. [[CrossRef](#)]
28. Bhakat, D.; Barik, P.; Bhattacharjee, A. Electrical conductivity behavior of Gum Arabic biopolymer-Fe<sub>3</sub>O<sub>4</sub> nanocomposites. *J. Phys. Chem. Solids* **2018**, *112*, 73–79. [[CrossRef](#)]
29. Luo, Q.; He, L.; Wang, X.; Huang, H.; Wang, X.; Sang, S.; Huang, X. Cyclodextrin derivatives used for the separation of boron and the removal of organic pollutants. *Sci. Total Environ.* **2020**, *749*, 141487. [[CrossRef](#)]
30. Mittal, H.; Morajkar, P.P.; Al Alili, A.; Alhassan, S.M. In-situ synthesis of ZnO nanoparticles using gum arabic based hydrogels as a self-template for effective malachite green dye adsorption. *J. Polym. Environ.* **2020**, *28*, 1637–1653. [[CrossRef](#)]
31. Renjini, M.; Bindhu, B. An in-depth study on the application of Gum Arabic: A Biopolymer. *Int. J. Recent Technol. Eng.* **2019**, *2019*, 1120–1121.
32. Birniwa, A.H.; Abdullahi, S.S. Study on physico-mechanical behaviour of acacia nilotica (gum tree) and glass fiber blend reinforced epoxy resin composite. *ChemSearch J.* **2019**, *10*, 46–53.
33. Mcnamee, B.F.; O’Riorda, E.D.; O’Sullivan, M. Emulsification and microencapsulation properties of gum arabic. *J. Agric. Food Chem.* **1998**, *46*, 4551–4555. [[CrossRef](#)]
34. Jagaba, A.H.; Kutty, S.R.M.; Noor, A.; Isah, A.S.; Lawal, I.M.; Birniwa, A.H.; Usman, A.K.; Abubakar, S. Kinetics of Pulp and Paper Wastewater Treatment by High Sludge Retention Time Activated Sludge Process. *J. Human Univ. Nat. Sci.* **2022**, *49*, 242–251.
35. Roque, A.C.; Bicho, A.; Batalha, I.L.; Cardoso, A.S.; Hussain, A. Biocompatible and bioactive gum Arabic coated iron oxide magnetic nanoparticles. *J. Biotechnol.* **2009**, *144*, 313–320. [[CrossRef](#)]

36. Yaro, N.; Napiyah, M.; Sutanto, M.; Usman, A.; Jagaba, A.; Mani, A.; Ahmad, A. Geopolymer utilization in the pavement industry-An overview. In Proceedings of the IOP Conference Series: Earth and Environmental Science, Zhuhai, China, 19–21 November 2022; IOP Publishing: Bristol, UK, 2022; p. 012025.
37. Birniwa, A.H.; Abdullahi, S.S.; Yakasai, M.Y.; Ismaila, A. Studies on physico-mechanical behaviour of kenaf/glass fiber reinforced epoxy hybrid composites. *Bull. Chem. Soc. Ethiop.* **2021**, *35*, 171–184. [[CrossRef](#)]
38. Roque, A.C.A.; Wilson, O.C., Jr. Adsorption of gum Arabic on bioceramic nanoparticles. *Mater. Sci. Eng. C* **2008**, *28*, 443–447. [[CrossRef](#)]
39. Sayed, K.; Baloo, L.; Kutty, S.R.B.; Al Madhoun, W.; Kankia, M.U.; Jagaba, A.H.; Singa, P.K. Optimization of palm oil mill effluent final discharge as biostimulant for biodegradation of tapis light crude petroleum oil in seawater. *J. Sea Res.* **2022**, *188*, 102268. [[CrossRef](#)]
40. Banerjee, S.S.; Chen, D.H. Fast removal of copper ions by gum arabic modified magnetic nano-adsorbent. *J. Hazard. Mater.* **2007**, *147*, 792–799. [[CrossRef](#)]
41. Birniwa, A.H.; Mahmud, H.N.M.E.; Abdullahi, S.S.; Habibu, S.; Jagaba, A.H.; Ibrahim, M.N.M.; Ahmad, A.; Alshammari, M.B.; Parveen, T.; Umar, K. Adsorption Behavior of Methylene Blue Cationic Dye in Aqueous Solution Using Polypyrrole-Polyethylenimine Nano-Adsorbent. *Polymers* **2022**, *14*, 3362. [[CrossRef](#)]
42. Farooq, M.; Sagbas, S.; Sahiner, M.; Siddiq, M.; Turk, M.; Aktas, N.; Sahiner, N. Synthesis, characterization, and modification of Gum Arabic microgels for hemocompatibility and antimicrobial studies. *Carbohydr. Polym.* **2017**, *156*, 380–389. [[CrossRef](#)]
43. Horst, M.F.; Coral, D.F.; van Raap, M.B.F.; Alvarez, M.; Lassalle, V. Hybrid nanomaterials based on gum Arabic and magnetite for hyperthermia treatments. *Mater. Sci. Eng. C* **2017**, *74*, 443–450. [[CrossRef](#)]
44. Nasef, S.M.; Badawy, N.; Hafez, F.; Slim, S.; El Nesr, E.M. Preparation and characterization of magnetic nanocomposite based on gum arabic/2-hydroxyethylmethacrylate using gamma irradiation for use in biomedical application. *Arab J. Nucl. Sci. Appl.* **2019**, *52*, 209–226. [[CrossRef](#)]
45. Ghaleb, A.; Kutty, S.; Ho, Y.; Jagaba, A.; Noor, A.; Al-Sabaeei, A.; Kumar, V.; Saeed, A. Anaerobic co-digestion for oily-biological sludge with sugarcane bagasse for biogas production under mesophilic condition. In Proceedings of the IOP Conference Series: Materials Science and Engineering, Ulaanbaatar, Mongolia, 10–13 September 2020; IOP Publishing: Bristol, UK, 2020; p. 012084.
46. Chockalingam, A.M.; Babu, H.K.R.R.; Chittor, R.; Tiwari, J.P. Gum arabic modified Fe<sub>3</sub>O<sub>4</sub> nanoparticles cross linked with collagen for isolation of bacteria. *J. Nanobiotechnology* **2010**, *8*, 1–9. [[CrossRef](#)]
47. Omer, A.M.; Dey, R.; Eltaweil, A.S.; Abd El-Monaem, E.M.; Ziora, Z.M. Insights into recent advances of chitosan-based adsorbents for sustainable removal of heavy metals and anions. *Arab. J. Chem.* **2022**, *15*, 103543. [[CrossRef](#)]
48. Saeed, A.A.H.; Harun, N.Y.; Sufian, S.; Bilad, M.R.; Zakaria, Z.Y.; Jagaba, A.H.; Ghaleb, A.A.S.; Mohammed, H.G. Pristine and magnetic kenaf fiber biochar for Cd<sup>2+</sup> adsorption from aqueous solution. *Int. J. Environ. Res. Public Health* **2021**, *18*, 7949. [[CrossRef](#)]
49. Movasaghi, Z.; Yan, B.; Niu, C. Adsorption of ciprofloxacin from water by pretreated oat hulls: Equilibrium, kinetic, and thermodynamic studies. *Ind. Crops Prod.* **2019**, *127*, 237–250. [[CrossRef](#)]
50. Alzahrani, E. Gum Arabic-coated magnetic nanoparticles for methylene blue removal. *Int. J. Innov. Res. Sci. Eng. Technol.* **2014**, *3*, 15118–15129. [[CrossRef](#)]
51. Jagaba, A.H.; Kutty, S.R.M.; Noor, A.; Birniwa, A.H.; Affam, A.C.; Lawal, I.M.; Kankia, M.U.; Kilaco, A.U. A systematic literature review of biocarriers: Central elements for biofilm formation, organic and nutrients removal in sequencing batch biofilm reactor. *J. Water Process Eng.* **2021**, *42*, 102178. [[CrossRef](#)]
52. Al-dhawi, B.N.S.; Kutty, S.R.M.; Baloo, L.; Almahbashi, N.M.Y.; Ghaleb, A.A.S.; Jagaba, A.H.; Kumar, V.; Saeed, A.A.H. Treatment of synthetic wastewater by using submerged attached growth media in continuous activated sludge reactor system. *Int. J. Sustain. Build. Technol. Urban Dev.* **2022**, *2022*, 2–10.
53. Jagaba, A.H.; Kutty, S.R.M.; Baloo, L.; Noor, A.; Abubakar, S.; Lawal, I.M.; Umaru, I.; Usman, A.K.; Kumar, V.; Birniwa, A.H. Effect of hydraulic retention time on the treatment of pulp and paper industry wastewater by extended aeration activated sludge system. In Proceedings of the 2021 Third International Sustainability and Resilience Conference: Climate Change, Virtual Event, 15–16 November 2021; IEEE: New York, NY, USA, 2021; pp. 221–224.
54. Mohammad, R.E.A.; Elbashir, A.A.; Karim, J.; Yahaya, N.; Rahim, N.Y.; Miskam, M. Adsorptive performances of magnetic graphene oxide adsorbent for the removal of fluoroquinolones in the Langat River Basin, Malaysia. *Int. J. Environ. Anal. Chem.* **2021**, *2021*, 1–20. [[CrossRef](#)]
55. Jagaba, A.H.; Kutty, S.R.M.; Hayder, G.; Baloo, L.; Noor, A.; Yaro, N.S.A.; Saeed, A.A.H.; Lawal, I.M.; Birniwa, A.H.; Usman, A.K. A systematic literature review on waste-to-resource potential of palm oil clinker for sustainable engineering and environmental applications. *Materials* **2021**, *14*, 4456. [[CrossRef](#)]
56. Jagaba, A.H.; Kutty, S.R.M.; Naushad, M.; Lawal, I.M.; Noor, A.; Affam, A.C.; Birniwa, A.H.; Abubakar, S.; Soja, U.B.; Abioye, K.J. Removal of nutrients from pulp and paper biorefinery effluent: Operation, kinetic modelling and optimization by response surface methodology. *Environ. Res.* **2022**, *214*, 114091. [[CrossRef](#)] [[PubMed](#)]
57. Khan, N.A.; Najam, T.; Shah, S.S.A.; Hussain, E.; Ali, H.; Hussain, S.; Shaheen, A.; Ahmad, K.; Ashfaq, M. Development of Mn-PBA on GO sheets for adsorptive removal of ciprofloxacin from water: Kinetics, isothermal, thermodynamic and mechanistic studies. *Mater. Chem. Phys.* **2020**, *245*, 122737. [[CrossRef](#)]

58. Mohammad, R.E.A.; Elbashir, A.A.; Karim, J.; Yahaya, N.; Rahim, N.Y.; Miskam, M. Deep Eutectic Solvent Functionalized Graphene Oxide Based Ferrofluid for the Liquid Phase Microextraction of Fluoroquinolones from Water Samples. *Key Eng. Mater.* **2022**, *920*, 114–121. [[CrossRef](#)]
59. Lawal, I.M.; Bertram, D.; White, C.J.; Jagaba, A.H.; Hassan, I.; Shuaibu, A. Multi-criteria performance evaluation of gridded precipitation and temperature products in data-sparse regions. *Atmosphere* **2021**, *12*, 1597. [[CrossRef](#)]
60. Wang, Y.; Lin, J.; Wang, Y.; Liu, Z.; Lian, J.; Liu, M. Highly efficient and selective removal of low-concentration antibiotics from aqueous solution by regenerable Mg(OH)<sub>2</sub>. *J. Environ. Sci.* **2020**, *87*, 228–237. [[CrossRef](#)] [[PubMed](#)]
61. Dong, L.; Shan, C.; Liu, Y.; Sun, H.; Yao, B.; Gong, G.; Jin, X.; Wang, S. Characterization and Mechanistic Study of Heavy Metal Adsorption by Facile Synthesized Magnetic Xanthate-Modified Chitosan/Polyacrylic Acid Hydrogels. *Int. J. Environ. Res. Public Health.* **2022**, *19*, 11123. [[CrossRef](#)] [[PubMed](#)]
62. Wang, S.; Liu, Y.; Yang, A.; Zhu, Q.; Sun, H.; Sun, P.; Yao, B.; Zang, Y.; Du, X.; Dong, L. Xanthate-Modified Magnetic Fe<sub>3</sub>O<sub>4</sub>@SiO<sub>2</sub>-Based Polyvinyl Alcohol/Chitosan Composite Material for Efficient Removal of Heavy Metal Ions from Water. *Polymers* **2022**, *14*, 1107. [[CrossRef](#)]
63. Jagaba, A.H.; Kutty, S.R.M.; Baloo, L.; Birniwa, A.H.; Lawal, I.M.; Aliyu, M.K.; Yaro, N.S.A.; Usman, A.K. Combined treatment of domestic and pulp and paper industry wastewater in a rice straw embedded activated sludge bioreactor to achieve sustainable development goals. *Case Stud. Chem. Environ. Eng.* **2022**, *6*, 100261. [[CrossRef](#)]
64. Alqadami, A.A.; Naushad, M.; Abdalla, M.A.; Ahamad, T.; AlOthman, Z.A.; Alshehri, S.M.; Ghfar, A.A. Efficient removal of toxic metal ions from wastewater using a recyclable nanocomposite: A study of adsorption parameters and interaction mechanism. *J. Clean. Prod.* **2017**, *156*, 426–436. [[CrossRef](#)]
65. Surgutskaia, N.S.; di Martino, A.; Zednik, J.; Ozaltin, K.; Lovecká, L.; Bergerová, E.D.; Kimmer, D.; Svoboda, J.; Sedlarik, V. Efficient Cu<sup>2+</sup>, Pb<sup>2+</sup> and Ni<sup>2+</sup> ion removal from wastewater using electrospun DTPA-modified chitosan/polyethylene oxide nanofibers. *Sep. Purif. Technol.* **2020**, *247*, 116914. [[CrossRef](#)]
66. Yin, D.; Xu, Z.; Shi, J.; Shen, L.; He, Z. Adsorption characteristics of ciprofloxacin on the schorl: Kinetics, thermodynamics, effect of metal ion and mechanisms. *J. Water Reuse Desalin.* **2018**, *8*, 350–359. [[CrossRef](#)]
67. Hu, Y.; Pan, C.; Zheng, X.; Liu, S.; Hu, F.; Xu, L.; Xu, G.; Peng, X. Removal of ciprofloxacin with aluminum-pillared kaolin sodium alginate beads (CA-Al-KABs): Kinetics, isotherms, and BBD model. *Water* **2020**, *12*, 905. [[CrossRef](#)]
68. Khoshnamvand, N.; Ahmadi, S.; Mostafapour, F.K. Kinetic and isotherm studies on ciprofloxacin an adsorption using magnesium oxide nanoparticle. *J. Appl. Pharm. Sci.* **2017**, *7*, 079–083.
69. Ullah, A.; Zahoor, M.; Alam, S. Removal of ciprofloxacin from water through magnetic nanocomposite/membrane hybrid processes. *Desalin. Water Treat.* **2019**, *137*, 260–272. [[CrossRef](#)]
70. Saeed, A.A.H.; Harun, N.Y.; Sufian, S.; Ghaleb, A.A.S.; Jagaba, A.H.; Mohammed, H.G.; Abdulrab, H.Q.A. Removal of Cadmium (II) from Aqueous Solution by Rice Husk Waste. In Proceedings of the 2021 International Congress of Advanced Technology and Engineering (ICOTEN), Virtual Event, 4–5 July 2021; IEEE: New York, NY, USA, 2021; pp. 1–6.
71. Khokhar, T.S.; Memon, F.N.; Memon, A.A.; Durmaz, F.; Memon, S.; Panhwar, Q.K.; Muneer, S. Removal of ciprofloxacin from aqueous solution using wheat bran as adsorbent. *Sep. Sci. Technol.* **2019**, *54*, 1278–1288. [[CrossRef](#)]
72. Cheng, R.; Li, H.; Liu, Z.; Du, C. Halloysite nanotubes as an effective and recyclable adsorbent for removal of low-concentration antibiotics ciprofloxacin. *Minerals* **2018**, *8*, 387. [[CrossRef](#)]
73. Zaman, H.G.; Baloo, L.; Kutty, S.R.; Altaf, M. Post Synthetic Modification of NH<sub>2</sub>-(Zr-MOF) via Rapid Microwave-Promoted Synthesis for Effective Adsorption of Pb (II) and Cd (II). *Arab. J. Chem.* **2022**, *15*, 104122. [[CrossRef](#)]
74. Duran, H.; Yavuz, E.; Sismanoglu, T.; Senkal, B. Functionalization of gum arabic including glycoprotein and polysaccharides for the removal of boron. *Carbohydr. Polym.* **2019**, *225*, 115139. [[CrossRef](#)] [[PubMed](#)]
75. Baloo, L.; Isa, M.H.; Sapari, N.B.; Jagaba, A.H.; Wei, L.J.; Yavari, S.; Razali, R.; Vasu, R. Adsorptive removal of methylene blue and acid orange 10 dyes from aqueous solutions using oil palm wastes-derived activated carbons. *Alex. Eng. J.* **2021**, *60*, 5611–5629. [[CrossRef](#)]
76. Afolabi, H.K.; Nasef, M.M.; Nordin, N.A.H.M.; Ting, T.M.; Harun, N.Y.; Abbasi, A. Facile preparation of fibrous glycidol-containing adsorbent for boron removal from solutions by radiation-induced grafting of poly (vinylamine) and functionalisation. *Radiat. Phys. Chem.* **2021**, *188*, 109596. [[CrossRef](#)]